学位論文（要約）

Numerical and experimental studies of ice lens formation with implication for interfacial melting

（アイスレンズ形成に関する数値的・実験的研究と界面融解への推察）

平成26年12月博士（理学）申請

東京大学大学院理学系研究科

地球惑星科学専攻

猿谷　友孝

ABSTRACT

When a homogeneous mixture of water and granular materials are frozen, pure ice layers known as ice lens are segregated out. They are formed by the migration and solidification of unfrozen water that is adsorbed to particle surface and confined to capillary regions. Growth of ice lens is responsible for the upwards displacement of the ground surface known as frost heave. The complicated interplay between heat and mass transport that causes ice lens formation and frost heave has been addressed by several theoretical models, but uncertainties still remain and require further experimental constraints and comparisons. Especially, the subject about the initiation of ice lenses has been remained uncertain because of the difficulty in theoretical treatment.

I performed a series of step-wise freezing experiments to observe the initiation and growth of ice lenses in fine granular materials. Freezing experiments demonstrate the clear relationships between the behavior of ice lenses, and the host particle size and the induced cooling temperature. Ice lenses are thicker with smaller particle sizes and the initial formation position is further from the cooled boundary with lower cooling temperatures. I compared the experimental results to numerical predictions of ice lens formation that are applied to the experimental conditions. Comparisons between the numerical predictions and experimental results emphasize the importance of water flow through the liquid thin film and suggest premelting in my experimental system is dominated by short-range electrostatic interactions. Particle size control based on the effective Peclet number indicates that ice lens growth in fine-grained porous media is constrained by low permeability in unfrozen region; by contrast, the restriction of thin film flow constrains the lens growth in coarse-grained porous media. Therefore, the ice lens growth is controlled by the balance between permeable flow and thin film flow, which leads to the high frost-susceptibility at intermediate-sized porous media. Beyond the fundamental experiments, I investigated the effect of salt on the initiation and growth of ice lenses and the redistribution during unidirectional freezing. The nucleated position of ice lenses and final location of solidification front are displaced to lower temperature side associated with the solute rejection from solid ice phase.

The physical model can explain the vigorous frost heaving in the fine-grained soils that has been indicated by previous field survey, but the model predicts smaller frost heave at further smaller particle size. The model also proposes the importance of packing conditions and size distributions that are intrinsic in natural system. When assessing and predicting the susceptibility for frost heave in particular natural system including extraterrestrial phenomena, the physical model can be applied to the intrinsic situations.

ACKNOWLEDGEMENT

I acknowledge Professor Kei Kurita of Earthquake Research Institute, University of Tokyo for supervising this study. Associate professor Alan W. Rempel in University of Oregon gave advice about numerical calculations and vigorous discussion. He gave me an opportunity to visit University of Oregon. Doctor Satoshi Akagawa in Hokkaido University assisted in making of sliced ice and polarization observations. I also would like to thank Mr. Masayuki Uchida in Laboratory for Technical Service and Development, Earthquake Research Institute for his help in making the experimental equipment of my research. Part of experiments and polarization observations were conducted in Institute of Low Temperature Science, Hokkaido University using collaboration research system. Associate professor Hidekazu Tanaka helped the working and discussion.

This work was supported by a grant for the Global COE Program, From the Earth to Earths, from the Ministry of Education, Culture, Sports, Science and Technology of Japan for the participation to international conference and internship to University of Oregon. Life in Earthquake Research Institute is supported by many colleagues, in particular, Mr. Ryuichi Nishiyama and Ms. Rina Noguchi helped me in my life. Finally I would like to show my gratitude to the family for their livelihood support.

Contents

1 Introduction **1**

1.1 Ice Lens Formation 1

1.2 Geophysical and Environmental Phenomena 2

1.3 Outline 4

2 Review of Ice Lens Formation and Frost Heave **6**

2.1 Overview of This Chapter 6

2.2 Ice Lens Formation and Frost Heave 7

2.3 Historical Sketch 7

2.3.1 Two Pioneers of Frost Heave Study 7

2.3.2 Theoretical Approaches 8

2.3.3 Experimental Approaches 10

2.4 Problems on Ice Lenses Studies 11

3 Review of Premelting Dynamics **16**

3.1 Overview of This Chapter 16

3.2 Intermolecular and Inter-particle Interaction 18

3.2.1 Intermolecular Interaction 18

3.2.2 Inter-particle Interaction 18

3.3 Liquid Thin Film 19

3.3.1 Surface and Interfacial Melting 19

3.3.2 Equilibrium Thickness of Liquid Thin Film 21

3.3.3 Measured Thickness of Liquid Thin Film 23

3.3.4 Amount of Unfrozen Water 24

3.4 Particle Rejection and Trapping 25
3.4.1 Thermal Regelation 25
3.4.2 Dependence on Particle Size and Freezing Rate 26
3.5 Colloidal System and Electrical Interaction 27
3.5.1 Debye length 27
3.5.2 Disjoining Pressure 27

4 Freezing Experiments **39**
4.1 Overview of This Chapter 39
4.2 Experimental Samples 40
4.2.1 Physical Properties of Granular Materials 40
4.2.2 Packing Conditions 40
4.3 Experimental Procedure 40
4.3.1 Experimental Setup 40
4.3.2 Freezing Experiments 41
4.4 Experimental results 41
4.4.1 Direct Observation of Ice Lens Growth 41
4.4.2 Configurations of Ice Lenses 42
4.4.3 Initiation and Growth of Ice Lenses 42
4.5 Additional Experiments 43

5 Modeling and Numerical Calculations **54**
5.1 Overview of This Chapter 54
5.2 Temperature Variations 56
5.3 Film Thickness 59
5.4 Continuum Force-balance Model 60
5.4.1 Hydrodynamic Pressure 60
5.4.2 Thermomolecular and Overburden Pressure 61
5.4.3 Lubrication Flow 62
5.5 Initiation and Growth of Ice Lenses 63
5.5.1 Initiation and Growth of Ice Lens 63
5.6 Dimensionless Parameters 65
5.6.1 Pelcet Number and Stefan Number 65

5.6.2 Particle Size Dependence 67

6 Overall Discussion **76**

6.1 Comparison between the Numerical Predictions and Experiments 76

6.1.1 Ice Lenses behaviors and Nature of Interactions 76

6.1.2 Implication for Nano-film Thickness 77

6.2 Structures of Ice Lenses 79

6.3 Geophysical Applications 80

6.3.1 Terrestrial Frost Heave Phenomena 80

6.3.2 Martian Ice Lenses 81

7 Conclusions **88**

A Numerical Calculations **94**

A.1 Discretization of Thermal Diffusive Equation 94

A.2 Dimensionless Equation 95

A.3 Sample Calculation 96

B Preliminary Experiments **99**

B.1 Temperature variations 99

B.2 Initiation and Growth of Ice Lenses 100

C Salt Effect **103**

C.1 Salt in Water 103

C.2 Salty Ice Lens Experiments 104

C.3 Experimental Results 104

C.3.1 Configurations of Salty Ice Lenses 104

C.3.2 Initiation and Growth of Salty Ice Lenses 105

C.3.3 Distributions of Electrolytes 105

D Analogy to Partial Melt **112**

D.1 Horoman Peridotite Complex 112

D.2 Possible Link between Ice Lens and Horoman Peridotite Complex 113

List of Tables

3.1 Hamaker constants 29
3.3 Characteristic energy scale 30

A.1 Calculation parameters 98

List of Figures

1.1 Visual table of contents 5

2.1 Unfrozen water in porous media 12
2.2 Taber's experiment 13
2.3 Frozen fringe 14
2.4 Various ice lenses 15

3.1 Characteristic energy scale 31
3.2 Molecular dynamics and ice surface melting 32
3.3 Diagram of interfacial melting 32
3.4 Spherical particle in ice 32
3.5 Thickness of unfrozen water 33
3.6 Amount of unfrozen water: I 34
3.7 Amount of unfrozen water: II 35
3.8 Amount of unfrozen water: III 36
3.9 Thermal regelation 36
3.10 Particle rejection and trapping 37
3.11 Critical freezing velocity 38

4.1 Measured porosity 45
4.2 Experimental setup 46
4.3 Diagram of solidification front advance 47
4.4 Successive images of ice lens growth 48
4.5 Frost heave and lens growth: II 49
4.6 Vertical cross sections of frozen samples 50

4.7 Main experimental results 51
4.8 Ice lenses in poly-dispersed glass beads 52
4.9 Ice lenses in basaltic soils 53

5.1 Partially frozen porous media 70
5.2 Coordinate system 71
5.3 Temperature variations 72
5.4 Ice-particle interface 72
5.5 Regime diagram of ice lenses 73
5.6 Kinetic effect 73
5.7 Diagram of lens initiation and freezing rate 74
5.8 Peclet number 74
5.9 Stefan number $\times$ Peclet number 75
5.10 Maximum growth rate 75

6.1 Comparison between numerical and experimental results 83
6.2 Inferred film thickness 84
6.3 Estimated location of ice lenses 85
6.4 Polarization images of ice lenses: I 86
6.5 Polarization images of ice lenses: II 87

A.1 Example of calculation 97

B.1 Location of solidification front 100
B.2 Preliminary experimental results 101
B.3 Frost heave and lens growth: I 102

C.1 Binary phase diagram of H_2O-NaCl system 107
C.2 Salty ice lenses images 108
C.3 Closeup images 109
C.4 Location of salty ice lenses 110
C.5 Estimated lens temperature 110
C.6 Concentration increase 111
C.7 Concentration distribution 111

D.1 Horoman peridotite complex 114
D.2 Grain boundary melting 115

Chapter 1

Introduction

1.1 Ice Lens Formation

When the mixture of water and fine particles are cooled below the melting temperature, segregated layers of pure ice are formed, which are called as *ice lenses*. The formation of ice lenses includes the migration and solidification of unfrozen water that is adsorbed to particle surfaces and confined to capillary regions and remains in liquid state below the nominal melting temperature. This behavior results from two distinct mechanisms: interfacial premelting associated with intermolecular forces such as van der Waals forces between ice, liquid and particles, and curvature-induced melting results from the interplay between the pore geometry and the surface energy of ice-liquid interface, which is referred to as the *Gibbs-Thomson* effect. Recently, the studies of ice lens and frost heave have been progressed by the development of *premelting dynamics* by J.G. Dash, M.G. Worster, J.S. Wettlaufer and A.W. Rempel. The fundamental of intermolecular interactions, premelting dynamics and its application are detailed in [Dash et al., 1995, Worster and Wettlaufer, 1999, Dash et al., 2006, Israelachvili, 2011, Rempel, 2012] . Although the formation of ice lens is macroscopic phenomenon within the millimeter scale, its fundamentals are microphysics of soils or fine-particles, and nano-scaled water flow through the liquid thin film as illustrated in Figure 1.1. Nano-scaled water behavior produces the various phenomena in diverse fields as described follows.

1.2 Geophysical and Environmental Phenomena

Ice lens growth in ground is responsible for upwards displacement of ground surface known as *frost heave*. Frost heave produces various types of periglacial landforms and causes serious damage to construction engineering [Beskow, 1935, Andersland and Ladanyi, 2004, French, 2007, Anderson and Anderson, 2010]. Over durations of months and years, formation of patterned ground associated with differential frost heave, and bedrock fracture by ice segregation are resulted [Werner and Hallet, 1993, Murton et al., 2006, Peterson and Krantz, 2003, 2008, Peterson, 2011]. For example, when the coarse and fine grains exist in a slope area, the formation of needle ice and frost heave prevail at fine-grained region, while coarse grains remain behind *in-situ*. This sorting leads to the differential frost heave and the formation of patterned ground. As for the engineering problems, the pipelines for gas and liquid transportation, constructions such as railway, paved road and buildings in cold region have been damaged by vigorous frost heaving for a long time. Therefore many constructions in cold region have been designed to restrict frost heaving. Ice lens formation and frost heave that includes water migration and redistribution are important processes in agriculture and vegetation because ice segregation in shallow ground surface causes various phenomena such as flow of surface soils associated with ice melting, break of plant root, or weakening of the ground.

Physical process in frozen soil and permafrost play an important role in climate change and global warming. Surface in cold region experiences the freeze-thaw effect; and active mass and heat transport between underground, surface and atmosphere. For example, release of gas such as carbon dioxide and methane, and flowage of water affect the vegetation, atmosphere and climate system. Therefore, the understanding of physical process in frozen soil is important for the prediction of climate change. Ice lens formation and frost heave that involve the mass and heat transport play a leading role in the cold region's physical process. Previous studies have adopted empirical models and macroscopic numerical models, while the empirical models are not based on the physics and numerical models are not supported by experimental proof. Insufficient understanding of the physical process in frozen soil may cause the uncertainties in the climate change predictions.

Beyond the terrestrial environment, similar processes are thought to occur on the Martian environment. Detailed exploration of Mars has yielded various direct and indirect ev-

idence of ice and ice-related landforms. HiRISE has observed various types of periglacial landform such as patterned ground, solifluction lobe and so on [e.g., Shean et al., 2005, Mellon et al., 2008, Levy et al., 2010]. In addition to the indirect evidence of ice, high-purity ice has been discovered at several cm below the ground surface by Phoenix lander at high latitude on Mars [Smith et al., 2009]. The existence of ice layer at near-surface is a challenge in the present martian environment. This pure ice is unlikely to be formed by the cold-trapping of atmospheric water vapor. Most likely origin of this ice is "segregated ice" which is also called ice lens [Mellon et al., 2009]. Sizemore et al. [2014] have developed a numerical model based upon the continuum model by Rempel et al. [2004] with martian climate model of Zent [2008] to track the initiation and growth in the martian environment. They indicated that ice lens nucleation is an ubiquitous process at high latitude, however, its growth magnitude depends on the soil properties strongly. If clay-sized particles or perchlorate salt exists in regolith, the ice lens growth becomes a vigorous process. However, more theoretical and experimental works are required to investigate the relation between the segregated ice and the excess ice at Phoenix landing site. In the future, the importance of unfrozen water will be recognized in the field of extraterrestrial environment, habitability and astrobiology, and premelting dynamics and its application will become key challenges.

Although the studies of ice lens and frost heave have long histories as described in following chapter 2, the whole pictures of the relevant physical processes are still unrevealed due to the complexity of phenomena and the lack of experimental constraints. Previous experiments are performed as a practical test so that the theoretical verification was not conducted. By contrast, the theoretical models are not based on the experimental verifications. Accordingly, the comparisons and integrations between the numerical predictions and experimental results are insufficient. Recently, fundamental processes of ice lens formation and frost heave have been better understood associated with the development of *Premelting dynamics* (details in chapter 3). In this thesis, I explore the formation mechanisms of ice lenses and resultant geophysical process by numerical simulation and freezing experiments.

1.3 Outline

In this thesis, chapter 2 reviews the historical sketch of ice lens and frost heave studies with focusing on the theoretical model of formation process and various freezing experiments. Chapter 3 describes the physical fundamentals about premelting dynamics. The intermolecular and inter-particle interactions, thickness and behavior of liquid thin film, particle rejection-trapping around solidification front, colloidal suspension and electrical interactions in water that are underlying basis of ice lens formation are detailed. Chapter 4 descries the freezing experiments about ice lens formation using homogeneous glass beads. I have performed systematic experiments with changing the cooling temperature and host particle size to observe the conditions and configuration of ice lens and to obtain the experimental constraints of the numerical models. In chapter 5, I have developed a simple model of ice lens initiation and growth based on the continuum model [Rempel et al., 2004] to compare with experimental results by solving the thermal diffusion equation in ice-water-particle system as moving boundary problem (i.e., Stefan problem). Chapter 6 describes the overall discussions. The comparisons between numerical predictions and experimental results are discussed. Beyond the ice lens behaviors, I have extended the objective to the interfacial melting and the nature of inter-particle interactions. Finally I discuss the geophysical applications. Chapter 7 describes the summary of this thesis and possible directions for future research.

Chapter 2

Review of Ice Lens Formation and Frost Heave

2.1 Overview of This Chapter

This chapter describes the history and previous studies of ice lenses and frost heave in theoretical and experimental approaches. In the theoretical approaches, I explain the some examples of previous models such as capillary model by Everett [1961], kinetic model by Kuroda [1985], rigid-ice model by O'Neill and Miller [1985], continuum force-balance model by Rempel et al. [2004] and crack-like model by Style et al. [2011] briefly. Within the various models, improvement of rigid-ice model is still continued by some researchers vigorously even now. Fundamental physics of ice lens formation is described in the following chapter 3. As for the experimental approaches, I introduce the previous freezing experiments performed by many researchers [e.g., Watanabe, 2002, Murton et al., 2006, Nagashima et al., 2008]. At last, I remark the problems to be solved on ice lenses and frost heave studies as a motivation to this thesis. They require the experimental comparisons and constraints against the numerical models.

2.2 Ice Lens Formation and Frost Heave

When the mixtures of water and soil grains are exposed to below the melting temperature, a pure ice layer is segregated out in frozen soils. This segregated ice layer is called as *ice lens*. Ice lens formation occurs not only in the system of water and soils grains but also in the system of liquid such as argon, helium, brine, with grains such as glass beads, clay, corn starch, bedrock, and other granular materials [Hiroi et al., 1989, Mashl et al., 1996, Watanabe and Mizoguchi, 2000, Zhu et al., 2000, Murton et al., 2006, Mizusaki et al., 2007, Nagashima et al., 2008, Peppin et al., 2008, Saruya et al., 2013]. Through freezing of porous media, the homogeneous mixtures of water saturated porous media are transformed to heterogeneous and multiphase structures. Initiation and growth of ice lenses cause the upwards displacement of ground surface known as *frost heave* and hence the formation of periglacial landforms. Since frost heaving damages the construction or railway, ice lens formation and frost heave have been studied from the engineering stand points. The formation mechanisms of ice lenses have long been investigated by many researchers [Everett, 1961, Gilpin, 1980, Kuroda, 1985, O'Neill and Miller, 1985, Wilen and Dash, 1995a, Worster and Wettlaufer, 1999, Rempel et al., 2004, Rempel, 2007, Style et al., 2011, Style and Peppin, 2012, Saruya et al., 2014b]. They have emphasized an important role of *premelting* or unfrozen water that is adsorbed to particle surface and confined to capillary regions in a porous media (see Figure 2.1). Unfrozen water remains in liquid state even below the nominal melting temperature. They result from intermolecular force and Gibbs-Thomson effect. The fundamental physics of unfrozen or *premelting* water and intermolecular and inter-particle interactions are described in chapter 3. In the following section, I describe the previous studies about ice lens and frost heave.

2.3 Historical Sketch

2.3.1 Two Pioneers of Frost Heave Study

Studies of ice lens formation and frost heave have a long history since Taber's pioneering experiments [Taber, 1929, 1930] (see Figure 2.2). He observed frost heave dynamics

using commercial refrigerator and recognized that the 10 % volume change between water and ice can not explain the magnitude of upwards displacement of surface. To survey the cost of frost damage to roads, constructions and railways, Beskow [1935] investigated the frost susceptibility by field observations. He noted that coarse grains such as sand or gravels rarely cause the surface displacement, however, silt-sized grains have high frost susceptibility. Studies by Taber and Beskow became the pioneers of ice lens and frost heave.

2.3.2 Theoretical Approaches

High frost-susceptibility of fine-grained particles draws researcher's attention to capillary phenomena. Everett [1961] modeled the mechanism of water drawing toward lens growth face based upon the surface tension effects. When the inter-particle pore is enough small, ice grows with rejecting soil particles. However, problems of the capillary theory have been pointed out by some researchers [e.g., Watanabe, 2002, Style and Peppin, 2012]. For example, the predicted maximum frost heave pressure and growth rate of ice lenses are much greater than the experimental predictions. Also the capillary model can not explain the periodic lenses, i.e., initiation of new lenses.

Kuroda [1985] focused on the chemical potential of water and modeled kinetic effect of ice lens growth. Chemical potential of liquid thin film adjacent to lens growth face is lower than that in pore water associated with the interaction with particle surface. Difference of the chemical potential drives the water flow to ice lens with balancing the increase of film thickness due to water adsorption and decrease of film due to freezing on lens. Therefore the growth rate of ice lens is proportional to the chemical potential difference and restricted by the resistance of water adsorption and freezing process.

Framework of recent studies of ice lens formation theories was constructed by the secondary frost heave model or rigid-ice model by O'Neill and Miller [e.g., Miller, 1972, 1978, O'Neill and Miller, 1985]. The suggested the existence of *frozen fringe* in frozen porous media that connects the solidification front and lens growth face (see Figure 2.3). In the frozen fringe, unfrozen water exists in particle surface and capillary region, and interstitial pore ice is connected as *rigid-ice* to ice lens. They focused on the stresses of each component and argued that ice lens nucleation occurs when the effective stress of

inter-particles becomes zero supported by ice and pore water. Subsequently, interstitial rigid-ice and particles move along the heat flow as *thermal regelation*. This model can explain the initiation of new lenses associated with a variations in effective stress through the advance of solidification front. However, the problems whether the frozen fringe exists or not still remain. Detection and optical inspection of frozen fringe is very difficult because typical pore space is micro-scale and the indices of refraction of water and ice are very close [Style and Peppin, 2012]. Although substantial experiments have been performed to detect the frozen fringe, this problem is not yet solved.

Dash and his colleagues have argued the mechanisms of dynamics of premelted water and ice lens formation based upon the intermolecular interactions between sediment particles [e.g., Dash, 1989, Dash et al., 1995, Wettlaufer and Worster, 1995, Wilen and Dash, 1995a, Wettlaufer et al., 1996, Worster and Wettlaufer, 1999, Rempel et al., 2001a]. Interfacial premelting is caused by intermolecular forces (such as van der Waals forces) between ice, water and particle. Intermolecular forces produce the net thermomolecular pressure that is responsible for particle migration. Wilen and Dash [1995a] observed the deflection of a flexible membrane in solidification experiments and indicated that thermomoelcular pressure gradient causes water flow in liquid thin film. Worster and Wettlaufer [1999] modeled a simple theory for steady-state ice lens growth with examining the force balance on a single particle. Particle migration due to thermomolecular pressure causes the water flow and hydrodynamic pressure gradient around particle surface. For ice lens to grow in a steady state, the pressures should be balanced. Details of *premelting dynamics* and thermomolecular pressure are described in chapter 3. Based on the "rigid-ice" model Rempel et al. [2004] developed a model that focuses on the force balance between sediment particles using a concept of thermomolecular pressure that is suggested by Dash and his colleagues. When the inter-particle pressure is unloaded by the balance of hydrodynamic pressure, overburden pressure and thermomolecular pressure, ice lens is nucleated. Details for this model are described in chapter 5.

Style et al. [2011] have suggested a crack-like model without frozen fringe. Ice lens nucleation starts from large pore in porous media due to geometrical supercooling and subsequently enlarges by a crack-like growth normal to the direction of heat flow. Thereafter, kinetics of ice lens growth has attracted attention by Style and Peppin [2012]. They have emphasized the flow resistance in the unfrozen region and liquid thin film

constrains the lens growth. Hydraulic resistance to flow in the unfrozen region restricts the lens growth in coarse grains; by contrast, interfacial resistance around particle surface restricts the growth in fined-grains. Subsequently, frost susceptibility maximizes in medium-grained soils.

2.3.3 Experimental Approaches

As described in the previous section, studies of ice lens and frost heave started with Taber's experiments [Taber, 1929, 1930]. Beyond water-soils system, frost heave experiments were performed using benzene and nitrobenzene that show volume reduction during the phase change from liquid to solid state. Since Taber's experiments, a number of freezing experiments have been performed. The main purpose of these experiments is to predict the amount of heaving and investigate the frost susceptibility of various soils because the damage of construction associated with frost heaving was a serious problem. Therefore these experiments are conducted in terms of engineering approaches including the development of frost heave test equipment. By contrast, observations of ice lenses have been performed in terms of physics and earth science. Figure 2.4 shows various types of ice lenses observed during freezing experiments: (a) periodic lenses (black band) in glass powder obtained by ramped freezing [Watanabe and Mizoguchi, 2000], (b) bedrock fracture due to ice segregation in a block of chalk [Murton et al., 2006], (c) layers of tetrahydrofuran clathrate hydrates in glass beads [Nagashima et al., 2008], (d) crack-like growth ice lens in freezing kaoline clay [Style et al., 2011], (e) ice lenses in a consolidated soil under extra loading [Azmatch et al., 2012] (f) macroscopic lens in fine glass beads [Saruya et al., 2014a]. These experiments have observed the growth of ice lenses, wguke engineering experiments have focused on the amount of upward displacement of sediment surface rather than the lensing process. For example, Konrad and Morgenstern [1981], Konrad [2005] defined the *segregation potential* that describes the velocity of water adsorption and the amount of heave using temperature gradient. Segregation potential is a specific parameter to soils and can be estimated from experiments (e.g., the porosity and the amount of unfrozen water). Although the segregation potential model can not predict the location and nucleated time of ice lenses, it can estimate the amount of frost heaving and water adsorption.

Freezing experiment is distinguished into two types; step-wise freezing and ramped freezing. In a step-wise freezing, the cooling temperature is kept through the experiments or reduced in a stepwise. By contrast, the freezing velocity is kept through the experiments in ramped freezing. Ramped freezing experiments using fine glass beads and natural soils were performed by Watanabe and his colleagues [e.g., Watanabe and Mizoguchi, 2000, Watanabe, 2002] (see in Figure 2.4 a). They have observed the spacing and thickness of periodic lenses with various freezing velocities. The thickness of each lenses becomes thinner with an increase of the freezing rate, while the spacing has no correlation with the freezing rate. By contrast, the temperature of lens growth surface decreases with an increase of the freezing rate. A similar experiment using colloidal dispersions were performed by Anderson and Worster [2012]. They have reported that the thickness and spacing of periodic ice banding decreases at higher freezing rates. Beyond the ice lenses, periodic layers of tetrahydrofuran clathrate hydrates in porous media are observed by Nagashima et al. [2008] (see Figure 2.4 c). Both the thickness and interval between neighboring layers decreased at higher freezing rates.

In addition to the soft porous media such as glass beads or soils, ice segregation in rigid bedrock was observed by Murton et al. [2006] (see Figure 2.4 b). They investigated the fracture of a chalk block that exposed to cycled temperature variation simulating seasonal thawing and freezing of in active layer and permafrost and found consistency in the depth and geometry of fractures between the laboratory experiments and arctic permafrost.

2.4 Problems on Ice Lenses Studies

As described above, many studies about ice lens and frost heave have been performed by many researchers using numerical and experimental methods. However, there still exist the problems that have to be solved: 1) lack of comparison between numerical predictions and experimental results focused on the ice lens configurations, 2) lack of experimental and optical observations of ice lens initiation and growth, 3) lack of experimental constraints for theoretical model, and 4) theoretical difficulties on ice lens initiation (not well discussed previously). To solve these problems, I investigate the mechanisms of ice lenses by freezing experiments and numerical modeling with focusing on the particle size and the growth velocity of solidification front in this thesis.

第２章の図はインターネット公表に関する同意が得られなかったため非公表

Chapter 3

Review of Premelting Dynamics

3.1 Overview of This Chapter

This chapter explains the fundamentals of ice lens and frost heave processes with focusing on the *Premelting dynamics* based upon Dash et al. [2006] and Israelachvili [2011]. To begin with, intermolecular and inter-particle interactions, and liquid thin film that constitute the physical basics of ice lensing are described.

The intermolecular force such as van der Waals forces make a large contribution to the macroscopic inter-particle interactions. Interactions between solid particles or ice-particle interfaces produce a liquid thin film even below the nominal melting temperature. Existence of liquid thin film between the substrate and ice or ice surface that resultants from inter-particle interactions, reduces the free energy of the system in comparison with ice-particle or ice-air interface. Equilibrium thickness can be estimated using the difference in *Gibbs* (or *Helmholtz*) free energy or chemical potential between the ice and liquid thin film. The amount of unfrozen water depends on the properties of soil particles, for example, the particle size that is known as Gibbs-Thomson effect. Examples of measured film thickness and amount of unfrozen water are shown in Figures. Subsequently, the interactions between the particle and the solidification front, thermal regelation and particle behaviors are described with a focus on the particle size and the freezing velocity. Thermal regelation is associated with the dependence of liquid thin film on local temperature, which induces water flow and particle migration for ice lens growth.

At last, I explain the colloidal systems and electrostatic interactions associated with

the electrolyte effect. In the system of water and very fine-grained particles, not only van der Waals forces but also electrolytes have great contribution to the inter-particle interactions that can be ignored in the air.

3.2 Intermolecular and Inter-particle Interaction

3.2.1 Intermolecular Interaction

Coulomb force and polarization force act between charged atoms and molecules, and between bipolar atoms and molecules. However, dispersion forces induced from instantaneous electrical fluctuation also act between neutral atoms and molecules. Since dispersion force acts without charged particles, it has great contributions to inter-particle adhesion, surface tension and phase change within total van der Waals forces. Beyond the intermolecular interactions, interactions between the materials can be estimated by assuming the additivity of intermolecular interactions since the materials are composed of atoms and molecules.

3.2.2 Inter-particle Interaction

Van der Waals forces that act between two contiguous semi-infinite bodies are caused by dispersion force. When two semi-infinite bodies are separated by a distance of *h*, this acting force per unit area becomes

$$F_v = \frac{A}{6\pi h^3}, \tag{3.1}$$

where *A* is Hamaker constant that indicates the strength of van der Waals interactions. When Hamaker constant is negative, repulsion force is induced. The magnitude and sign of Hamaker constant vary greatly depending on the electrical properties of interface component materials. Table 3.2 shows the examples of Hamaker constant at various interfaces obtained from Wilen et al. [1995b]. Hamaker constant at ice-water system is an order of magnitude smaller than other two planar system separated by water. There are other interactions that act between two substrates or particles other than van der Waals interactions. Figure 3.1 and Table 3.4 show the characteristic energy scales and formulae against the length scales. Here interfacial energies (solid lines) such as van der Waals energy for air and water with Hamaker constant $A = 10^{-19}$ and 10^{-21} J, long-ranged electrostatic energy, double layer energy for brine and water with Debye-length = 30 nm and 960 nm are plotted as functions of distance between two adjacent surfaces. Van der Waals (colloid)

３章の一部はインターネット公表に関する同意が得られなかったため非公表

spectroscopy method was applied by Sadtchenko and Ewing [2002], who measured the sums of the film thickness of surface melted layer against water vapor and interfacial film against germanium. Relationships between film thickness and temperature measured by various researchers are summarized by Sadtchenko and Ewing (see Figure 3.5). The gradient of this log-log plot indicates the nature of dominant interfacial interactions of film behavior ν; non-retarded van der Waals forces give $\nu = 3$, retarded van der Waals forces give $\nu = 4$, and different limits of electrostatic forces give $\nu \approx 2$ or 3/2. For example, Sadtchenko and Ewing [2002] report $\nu \sim 3$, whereas Gilpin [1980] experiment has $\nu \sim 2.4$. Due to the difficulty of interfacial melting measurement, large discrepancies still exist depending on the experiments. Especially, the measurement of film thickness near the bulk melting temperature is rare.

3.3.4 Amount of Unfrozen Water

Amount of premelted or unfrozen water highly depends on the temperature and surface properties of soils grains. Various measurement methods of unfrozen water in porous media or natural soils have been developed. For example, Ishizaki et al. [1996] measured the amount of unfrozen water and temperature dependence (which is called as unfrozen water curve) in porous silica glass using pulse nuclear magnetic resonance (NMR) that detects the variations of magnetic moment and field derived from water molecules spin. Figure 3.6 shows the amount of unfrozen water in porous silica glass characterized by pore diameters. Since nominal pore diameter is roughly comparable to particle size, the porous media that have small pore and particle can hold large amount of unfrozen water. Time domain reflectometry (TDR) that applies the difference in the specific heat between ice and water, and melting heat of ice, was developed by Spaans and Baker [1995]. Anderson and Morgenstern [1973] measured the amount of unfrozen water in various natural soils using isothermal calorimetry (see Figure 3.7). Fine-grained soils such as bentonite hold large amount of unfrozen water even –10 °C, while coarse grains such as basalt rarely have unfrozen water even at higher temperature.

When porous media is saturated with brine, the amount of unfrozen water increases in comparison with the media saturated with pure water. Watanabe [2002] measured the amount of unfrozen water in glass powder and natural soils that are saturated with solu-

tion using pulse NMR. Figure 3.8 shows the measured and calculated amount of unfrozen water in Fujinomori soil. The amount of unfrozen water increase with increasing concentration of NaCl.

3.4 Particle Rejection and Trapping

3.4.1 Thermal Regelation

When a substrate particle is surrounded by ice with a temperature gradient, the particle is moved to warmer side by a process of melting and refreezing, which known as *thermal regelation*. This phenomenon was recognized and modeled with wire regelation experiments by Gilpin [1979]. He observed the motion of a weighted wire through ice associated with pressure-induced regelation. If a particle is surrounded by ice through the liquid thin film, (see Figure 3.9) temperature gradient causes the migration of particle. The total free energy of ice-melt and melt-particle interface is less than that of ice-particle system as described in the previous section. The intermolecular forces that act between a particle and solid ice through the liquid thin film produce the net thermomolecular pressure p_T(d) that repels the particle from the ice, referred to as the *disjoining pressure*.

The total free energy of the system should be minimized so that the film thickness at equilibrium conditions is described as

$$\rho_i \mathcal{L} \frac{T_m - T}{T_m} = \gamma_{il} \mathcal{K} + p_T(d) \ , \tag{3.20}$$

where γ_{il} is the surface energy of the ice-liquid interface and $\mathcal{K}$ is a interface curvature. Since interfacial premelting is induced by a pressure difference between the ice and liquid melt phases, right-hand in equation (3.20) describes the pressure difference $\Delta P = p_i - p_l$ [Baker and Dash, 1989, Rempel et al., 2001a, 2004]. Functional dependence of thermomolecular pressure $p_T(d)$ on temperature is determined by the nature of dominant intermolecular forces that act between ice and particle. When non-retarded van der Waals forces dominate the interactions of system, themomolecular pressure is written as

$$p_T = \frac{A}{6\pi d^3} \tag{3.21}$$

where A is the effective Hamaker constant of the interface and d is the film thickness. Since film thickness becomes thinner at the colder side, thermomolecular pressure becomes strong. Subsequently, strong thermomolecular pressure at colder side pushes the particle to warmer side. To maintain the mass balance, liquid at the warmer side flows to the colder side through the liquid thin film. The latent heat that released associated with freezing at the colder side is consumed to melting the ice at the warmer side.

3.4.2 Dependence on Particle Size and Freezing Rate

Ice lens growth is progressed with particle rejection from the solidification front. Particle behaviors at the moving solidification front were observed by some researchers [e.g., Corte, 1962, Lipp and Körber, 1993, Mutou et al., 1998]. Corte [1962] proved two distinct types of behavior in a series of unidirectional freezing experiments using mineral particles as for the particle size and freezing rate. At a solidification front, particles are trapped within solid ice for larger particles and rapid freezing. On the other hand, for smaller particles and slower freezing, particles are pushed ahead from solidification front and accumulated to front. Similar experiments have been performed by Mutou et al. [1998] and Lipp and Körber [1993]. Figure 3.10 shows two distinct behaviors of particles depending on the freezing rate observed by Mutou et al. [1998]. When the freezing rate is slow (a), particles are rejected from and accumulated to the solidification front; by contrast, particles are trapped in the solid ice when the freezing rate is rapid (b). As for the particle size dependence on particle behaviors, Lipp and Körber [1993] investigated the critical freezing velocity of various sized particles (see Figure 3.11). Fine particles are rejected at higher freezing velocity, while critical freezing velocity for large particles is significantly decreased. Interaction between particle and solidification front is well investigated by theoretically [Worster and Wettlaufer, 1999, Rempel and Worster, 1999]. Thermomolecular pressure that acts as disjoining pressure between advancing solidification front (i.e., ice) and particle through the liquid thin film pushes the particle to unfrozen region. This behavior is fundamental for the ice lens nucleation.

However, when the porous media is saturated with solution or salty water, behavior of particles at the solidification front becomes complicated. Since the electrolyte and impurity are rejected from the solidification front, the electrolyte concentration becomes

higher at the front so that concentration gradient and the instability of water-ice interface are induced at the unfrozen region. Subsequently, particle clusters and electrolyte are not rejected but trapped in grain boundaries of polycrystalline ice. Details for salt effects are discussed in Appendix D.

3.5 Colloidal System and Electrical Interaction

3.5.1 Debye length

Fine particles such as colloid particles in water are accompanied by the surface charge due to electrolytes and ions, which are suspended in solvent without sedimentation. Electrical double layer formed by the adsorption of counterion (against surface charge) produces the important electrostatic interactions between colloidal particles. Effective range of electrostatic interactions, or attenuation distance of potential is characterized by Debye length shown as

$$\kappa^{-1} = \left(\frac{\epsilon \epsilon_0 k_b T}{e^2 \rho_\infty} \right)^{1/2} , \tag{3.22}$$

and the electrical potential is

$$\psi \sim \psi_0 \exp(-\kappa x) , \tag{3.23}$$

where e is the elementary charge, ψ is the potential, ϵ_0 and ϵ are the permittivity of free-space and material, k_b is the Boltzmann constant, T is the temperature and ρ_∞ is bulk concentration of ion. Therefore, the Debye length describes the e-folding distance of the electrical potential and equation (3.23) is known as *Debye-Hückel* equation when the potential ψ_0 is significantly low. The Debye length depends only on the solution properties, for example, in the case of NaCl, $1/\kappa \sim 30.4$ nm for 10^{-4} M, 0.96 nm for 0.1 M, 960 nm for pure water with pH7.

3.5.2 Disjoining Pressure

I consider the charged particle surface in fresh water without electrolytes (i.e., not solution). Counterions in water are drawn toward particle surface and induce the Stern layer. Beyond the Stern layer, counterions move apart from surface by thermal diffusion in the

diffuse layer. Distributions of counterions in the diffuse layer can be estimated by solving Poisson-Boltzmann equation

$$\frac{\mathrm{d}^2\psi}{\mathrm{d}x^2} = \frac{-Ze\rho(x)}{\epsilon\epsilon_0} = \frac{-Ze\rho_0}{\epsilon\epsilon_0}\mathrm{e}^{-Ze\psi/k_bT} \ . \tag{3.24}$$

where Z is the valence of the ions, ρ_0 and $\rho(x)$ are the ion density of mid-plane and position x. Solution of Poisson-Boltzmann equation is

$$\exp\left(-\frac{Ze}{k_bT}\psi\right) = \sec^2(\mathrm{K}x) \ . \tag{3.25}$$

where K is obtained by solving

$$\mathrm{K}\tan\left(\frac{\mathrm{K}d}{2}\right) = \frac{-Ze}{2k_bT}\frac{\sigma}{\epsilon\epsilon_0} \ . \tag{3.26}$$

Pressure that acts between two adjacent charged surface separated by distance d is shown as

$$P(d) = 2\epsilon\epsilon_0\left(\frac{k_bT}{Ze}\right)^2\mathrm{K}^2 \ . \tag{3.27}$$

When the interface separation (or film thickness) d is significantly larger than molecular dimensions and surface charge is high, the term of tangent in equation (3.26) tends to a limiting value of $\pi/2$ so that equation (3.26) becomes

$$P(d) = 2\epsilon\epsilon_0\left(\frac{\pi k_bT}{Ze}\right)^2 d^{-2} \ , \tag{3.28}$$

which is known as *Langmuir* equation and referred to as the disjoining pressure. The conversion from the disjoining pressure to the undercooling temperature is estimated through equations (3.18) or (3.19) so that $\Delta T \sim 1.1 \times 10^6 \ P(d)$. When the film thickness is greater than Debye length (i.e., the particle is far away from adjacent particle), this approximation is unable to be applied; instead, double-layer pressure is useful, which is described using exponential form.

Table 3.1: Hamaker constants from Wilen et al. [1995b]. Hamaker constant at ice-water system is an order of magnitude smaller than other two planar systems separated by water.

Interface	Hamaker constant (10^{-18} J)
ice–water–gold	1.573
gold–water–gold	250.96
ice–water–silicon	-1.66
silicon–water–silicon	119.7
ice–water–polystyrene	0.122
polystyrene–water–polystyrene	13.4
ice–water–polyvinylchloride	-0.13
polyvinylchloride–water–polyvinylchloride	12.22
ice–water–fused quartz	0.03
fused quartz–water–fused quartz	7.46
ice–water–sapphire	0.63
sapphire–water–sapphire	51.2

Table 3.3: Characteristic energy scales of various interactions [Israelachvili, 2011]. Van der Waals (air water), electrostatic and double layer energies are characterized by the distance between the two adjacent surfaces d. Van der Waals (colloid), gravity and capillary energies are characterized by radius of spherical grains R. Parameters and details are described in the text. $\mathcal{Z}$ in double layer energy indicates the interaction constant.

Type of energy	Formulae
van der Waals (air water)	$\frac{A}{12\pi d^2}$
van der Waals (colloid)	$\frac{AR}{12\pi h}$
gravity	mgR
capillary	$2\pi\gamma R$
electrostatic	$\epsilon\epsilon_0\left(\frac{\pi k_b T}{Ze}\right)d^{-1}$
double layer	$\left(\frac{\kappa}{2\pi}\right)\mathcal{Z}\mathrm{e}^{-\kappa d}$
thermal energy	$k_b T$

第３章の図はインターネット公表に関する同意が得られなかったため非公表

Chapter 4

Freezing Experiments

4.1 Overview of This Chapter

This chapter describes the freezing experiment to observe the conditions and configurations of ice lenses and frost heave. I have prepared the various sizes of mono-dispersed glass beads from 0.6 μm to 100 μm. Glass beads that are saturated with deionized-degassed water, are frozen from the bottom side under a constant cooling temperature using Peltier module. After 24 hours of cooling, the frozen sample was cut along the central vertical area to observe the position and thickness of ice lenses. As a result of systematic experiments, I found clear relationships between the host particle size, cooling temperature, and position and thickness of ice lenses. In smaller particles, ice lens nucleates at the lower side (i.e., near the cooling plate) and grows largely. The direct observation during freezing shows that the heaving of sediment surface occurs before the macroscopic lens nucleation, and the total heaving amount exceeds the thickness of the macroscopic lens. In addition to the fundamental experiments, some additional experiments for poly-dispersed glass beads mixtures and natural soils are shown.

4.2 Experimental Samples

4.2.1 Physical Properties of Granular Materials

Since ice lens formation is a complicated physical process that includes mass and heat transport, glass beads that have uniform properties are more favorable than natural soils that have vesiculated structures, especially, to test the effects of particle size on ice lens formation. Accordingly, I used mono-dispersed beads of soda lime glass with diameters of 0.6, 1.5, 5, 10, 18, 32, 50, 70, and 100 μm (Potters-Ballotini Co., Ltd and Admatechs Co., Ltd). The thermal conductivity and the heat capacity of glass are 837 J K^{-1} and 1.1 W m^{-1} K^{-1}, respectively, Bulk density is 2600 kg m^{-3}. Particle surface is smooth. The glass beads were saturated with deionized, degassed (by the depressurization method) water before the start of each experiment. By contrast, water includes various concentration of NaCl in the salty ice lens experiments that are discussed in Appendix D.

4.2.2 Packing Conditions

I have measured the porosity using centrifugal at each particle sizes. Figure 4.1 shows the measured porosities. The porosity ϕ ranged from 0.40 for the larger particles to 0.54 for the smallest ($\phi_{0.6} \approx 0.70$, $\phi_{1.5} \approx 0.60$, $\phi_5 \approx \phi_{10} \approx 0.45$, $\phi_{18} \approx \phi_{32} \approx \phi_{50} \approx 0.40$, where subscripts denote the particle size in microns). For the 0.6 and 1.5 μm cases, during sample preparation I added a drop of solute (sodium chloride, < 30 ppm) to the pore waters to reduce the Debye length and improve sedimentation. When the drop of solute is added in the water, the porosities of 0.6 and 1.5 μm particles decrease to 0.54 and 0.40, respectively.

4.3 Experimental Procedure

4.3.1 Experimental Setup

Figure 4.2 shows a schematic diagram of experimental setup. The cylindrical acrylic container has inner diameter of 46 mm (outer 50 mm), and length of $\sim$ 40 mm (for preliminary) and 80 mm (main). At first I tested short length ($\sim$ 40 mm) as preliminary

experiments to investigate the lensing trend. Details and results are described in Appendix B. Subsequently, main experiments were performed using long length ($\sim$ 80 mm); their results are used to compared with numerical calculations. The aluminum bottom plate is attached directly to the Peltier module used for cooling (Sensor Controls Co., Ltd. and Takagi Mfg. Co., Ltd.). The top and lateral boundaries are covered by styrofoam as a thermal insulator. Each sample was overlain by liquid to ensure hydrostatic conditions at the upper boundary.

4.3.2 Freezing Experiments

The initial temperature was uniform at approximately 18 °C through the sediment column. At the beginning of each experiment, the bottom temperature was lowered abruptly and kept constant. The total cooling time was 15 (preliminary) and 24 hours (main) in duration. After each experiment, the frozen samples were preserved in refrigerator and cut along a central vertical plane to observe and measure the interior configurations. Three experiments were performed for each set of conditions. Temperatures were measured using chromel-alumel thermocouples (absolute accuracy $\pm$ 0.3 °C) placed at 2.5 (preliminary) and 10 mm (main) intervals, with the lowermost thermocouple located at 3 mm above the cooling plate. To minimize the effects of side boundaries, temperature was measured along the center-line of the cell. During a subset of the specific experiments, successive images of ice lens growth were taken at 60 minutes intervals to observe lens growth visually in a low pressure chamber.

4.4 Experimental results

4.4.1 Direct Observation of Ice Lens Growth

Main experiments were conducted using the cylindrical acrylic container with 80 mm in length. Figure 4.4 shows successive images of ice lens growth at 6 hours intervals. The particle size is 5 μm and the cooling temperature is –5 °C. In this experiment, the sample container was set in a low-pressure chamber to eliminate condensation and obtain clearer images. The horizontal dark zone is the ice lens; its growth front advanced upwards with time. The ice lens separates a mixture of ice and particles below from water and particles

above. Temporal variations of sediment surface and macroscopic lens are shown in Figure 4.5. Panel (a) shows the heaving amount of sediment surface and growth of macroscopic ice lens. Heave of sediment begins before macroscopic ice lens is nucleated. After the macroscopic lens nucleation, heave rate and growth rate are comparable. Surface heaving slightly prior to macroscopic lens nucleation implies that frost heave can occur without large growth of ice lens. Furthermore, the magnitude of surface heaving is larger than the thickness of macroscopic lens. This suggests that further *invisible* lensing occurred below the visible lens. Lensing behavior, invisible lenses and measured temperatures using thermocouples are discussed in chapter 5.

4.4.2 Configurations of Ice Lenses

Figure 4.6 shows the vertical cross section through a frozen sample (the photograph is of a sample that was preserved in a freezer at –15 °C following an experiment). The horizontal dark zone indicates the ice lens and the white zones are mixtures of frozen pore ice and glass beads. The ice lens is convex upward with a curvature along the ice-lens surface of approximately 3 m^{-1}. The difference in lens position between the center and outer boundaries is approximately 2 mm, which is an order of magnitude smaller than the cell radius. The location of lower side of each ice lens varied with the host particle sizes, while upper boundaries are stable regardless of the particle size. This indicates the location of final freezing front and the temperature variation are independent of host particle size.

4.4.3 Initiation and Growth of Ice Lenses

I measured the thickness and position at the center of each visible ice lens after 24 hours cooling. As defined previously, the position of an ice lens is the distance between its lower boundary and the bottom cooling plate. The relationships between the nucleate location (position), growth (thickness) and particle sizes are shown in Figure 4.7. Figure 4.7 (a) shows the relationship between the host particle size and the positions of ice lenses for a fixed cooling temperature of –5 °C. There is a clear correlation that ice lens occurs at higher locations in samples with larger particle sizes. The relationship between particle size and ice-lens thickness for the same thermal conditions is shown in Figure 4.7 (b) (cooling time 24 hours). The ice lens that formed in 0.6 μm particles is thickest, and

thinner lenses are developed in larger particles. As seen in Figure 4.6 ice lens with particle size of 50 μm looks like thin line.

High frost susceptivity (i.e., vigorous growth of ice lenses) of smaller particles is consistent with Beskow's early field observations. Gibbs–Thomson effect describes how the onset of freezing is depressed from the nominal bulk melting temperature. Assuming that the largest pore throats are comparable to the particle radius R, Gibbs-Thomson relation (3.11) predicts that ΔT_f for the warmest pore ice is 80 times larger for the 0.6 μm particles ($\Delta T_f \approx 0.2\,\mathrm{K}$) than for the 50 μm particles ($\Delta T_f \approx 0.002\,\mathrm{K}$). The fraction of the pore space occupied by unfrozen water decreases at colder temperatures [Cahn et al., 1992, Ishizaki et al., 1996] so that the permeability to water transport decreases rapidly and becomes negligible once the temperature depression reaches several times of ΔT_f [Andersland and Ladanyi, 2004, Rempel, 2012].

4.5 Additional Experiments

In addition to the simple experiments described above, I performed the freezing experiments with different internal factors. Figure 4.8 shows the ice lens in poly-dispersed glass beads. The upper panel is a mixture of 5 μm and 50 μm particles (mass ratio is 4 : 6) and the lower panel is of 5 μm and 1000 μm (mass ratio is 4 : 6). Measured porosity of poly-dispersed glass beads is ~ 0.32 and ~ 0.19 for 5-50 μm and 5-1000 μm, respectively. In both cases, ice lenses grow macroscopically despite the presence of large particles. Ice lenses in basaltic soils that have a large size distribution are shown in Figure 4.9. The particle diameter ranges from 125 to 425 μm at upper panel and 1000–4000 μm at lower panel, respectively. In both cases, the macroscopic lenses are formed despite the presence of large particles. This means that the small particles or microstructures plays a leading role in the growth of ice lens.

As for the salt effect in the ice lens formation, details are described in Appendix D. When the electrolytes and solution are included in the pore water, the melting temperature of water and electrostatic interactions between particles change with the salt concentration. Salty lens experiments conducted here demonstrate the substantial differences against the pure water experiments. When the salt concentration is high, ice lens becomes vague and large amount of particle clusters are not rejected from solidification front, but

trapped within the ice grain boundaries. As for the initiation and growth, the nucleated position shits lower side with the increase of salt concentrations, while the growth thickness is independent on the concentration. Measurements of concentration distribution after unidirectional freezing exhibit the condensation of solute at the solidification front.

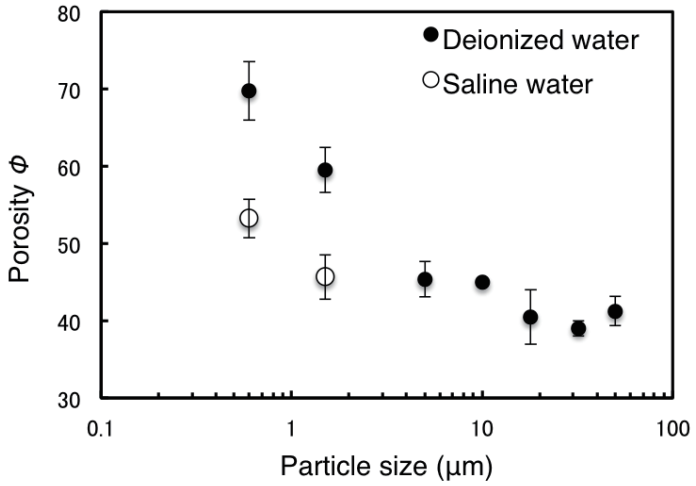

Figure 4.1: Measured porosity using weak centrifugal. The porosity ranges from 0.40 for the larger particles to 0.70 for the smallest particles (filled circles). When drop of solute is added to 0.6 and 1.5 μm particles, the porosities of 0.6 and 1.5 μm particles decrease to 0.54 and 0.40, respectively (open circles).

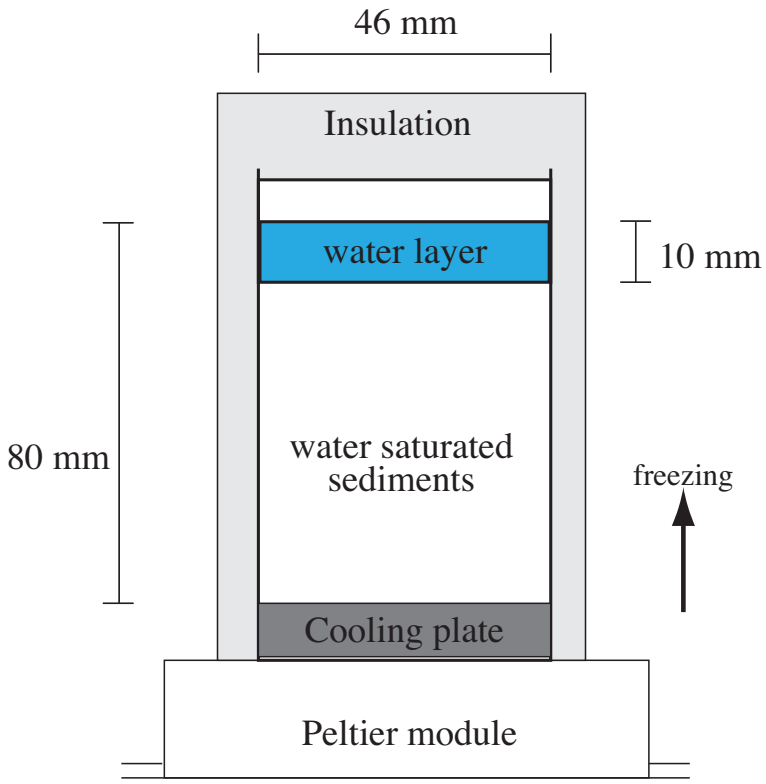

Figure 4.2: Schematic diagram of the experimental setup. Water-saturated glass beads are covered by 10 mm water layer. The aluminum bottom plate is directly attached to the Peltier module.

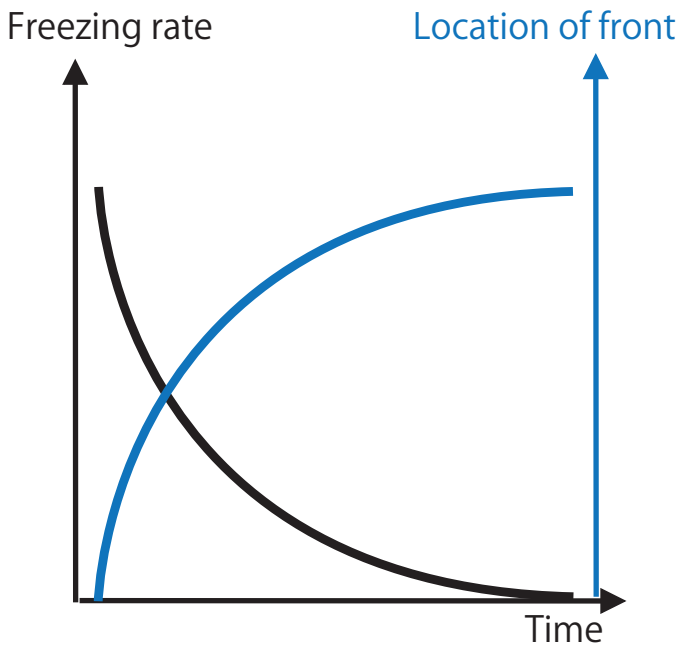

Figure 4.3: Relationship diagram between the freezing rate and its location during stepwise freezing. With the advance of solidification front upwards, the freezing rate becomes slow and stops.

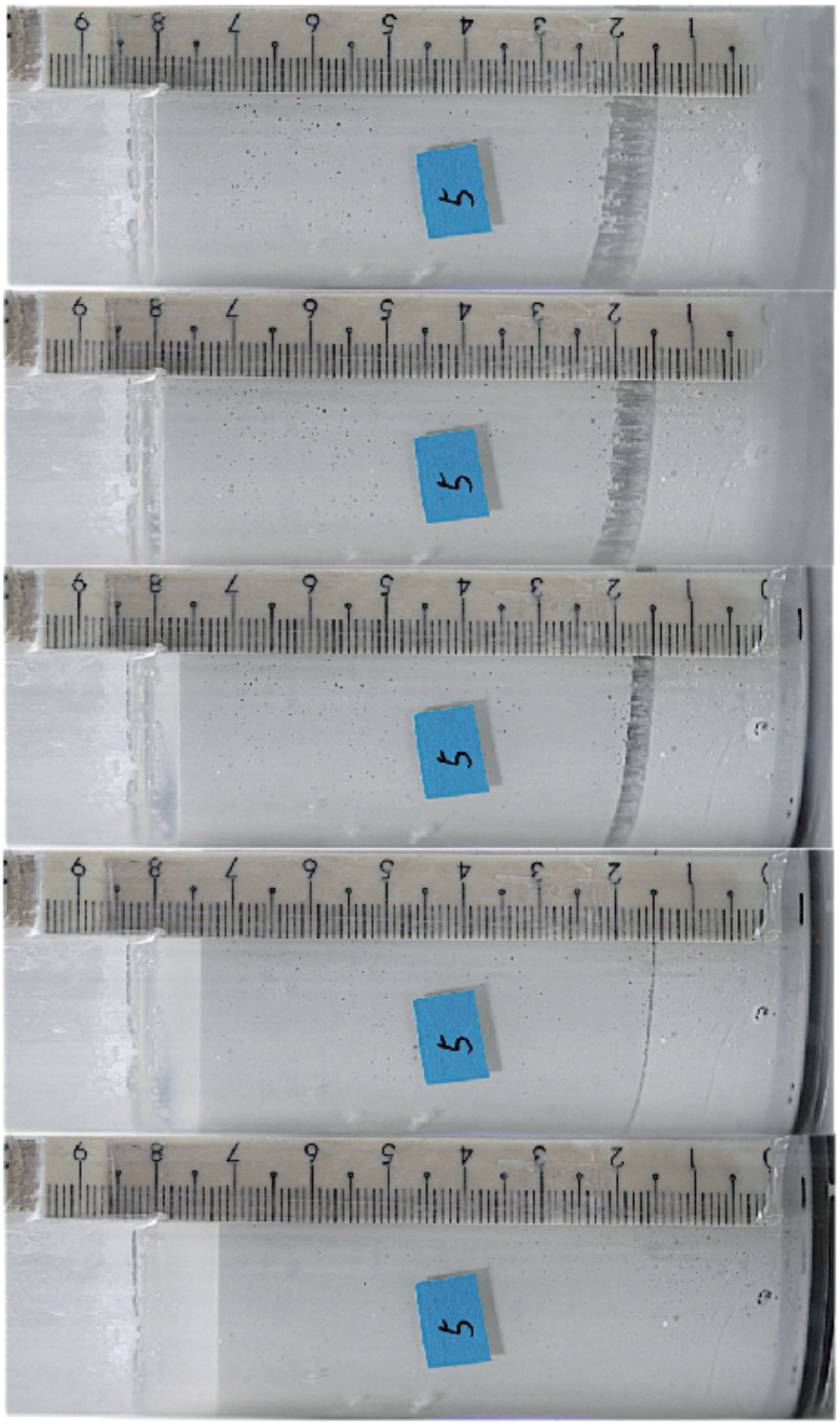

Figure 4.4: Successive images of ice lens growth at particle size of 5 µm and cooling temperature of –5 °C. Not only the ice lens growth, but also the surface of sediment heaves.

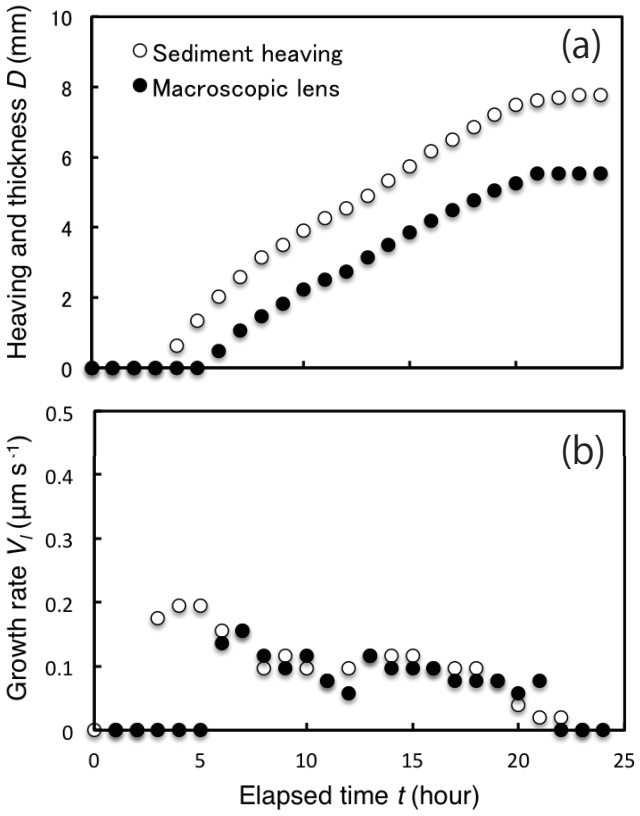

Figure 4.5: Frost heave and lens growth (a) Measured surface heaving (open circles) and macroscopic lens growth (filled circles) with particle size of 5 μm and cooling temperature of –5 °C obtained by main experiments. (a) heave of sediment surface begins before macroscopic lens is nucleated. (b) after macroscopic lens nucleation, sediment heave rate and lens growth rate are comparable.

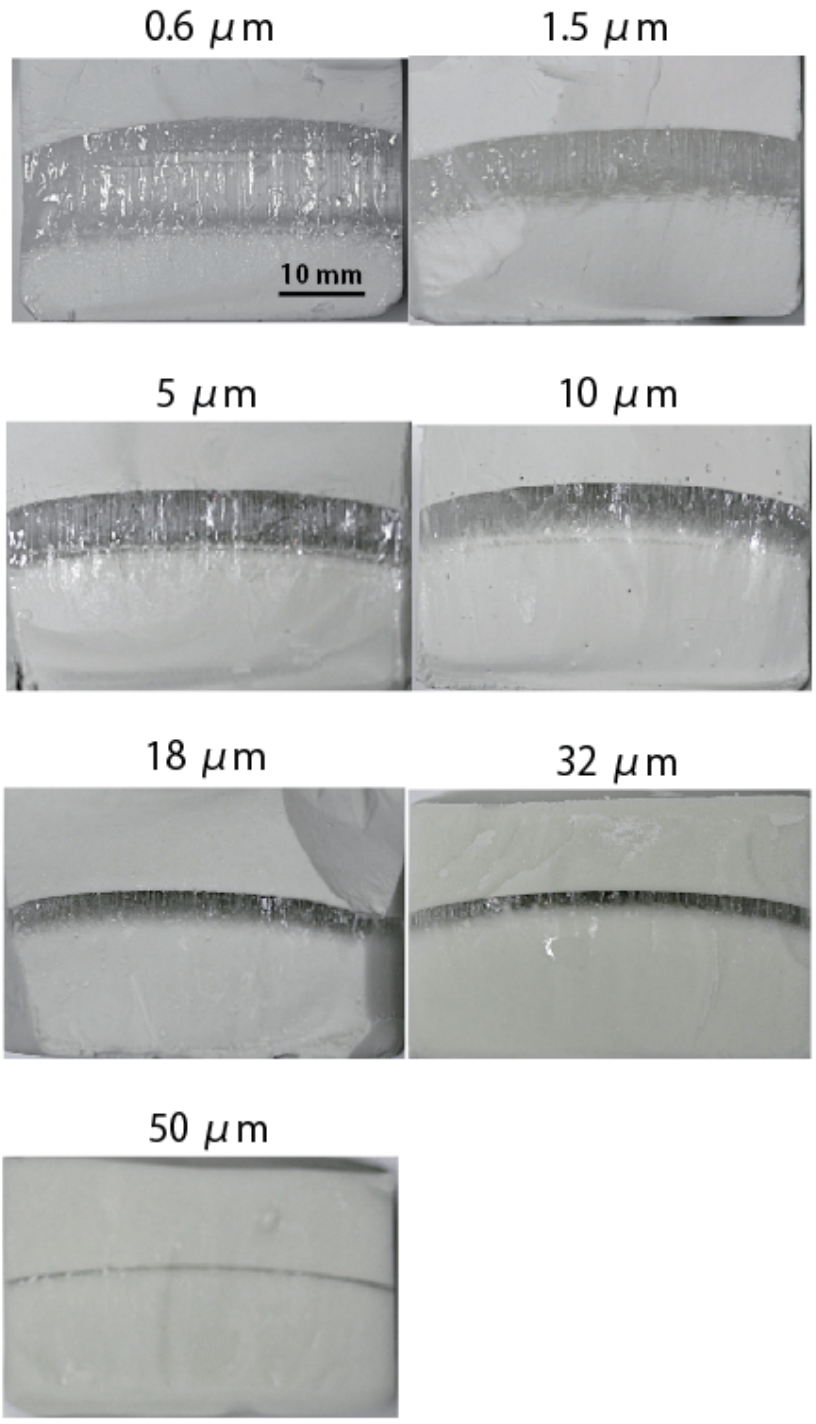

Figure 4.6: Central vertical sections of frozen samples at different particle sizes. The horizontal dark zone is the ice lens and the white zone are mixtures of frozen pore ice and glass beads. The ice lenses have a convex-upward shape.

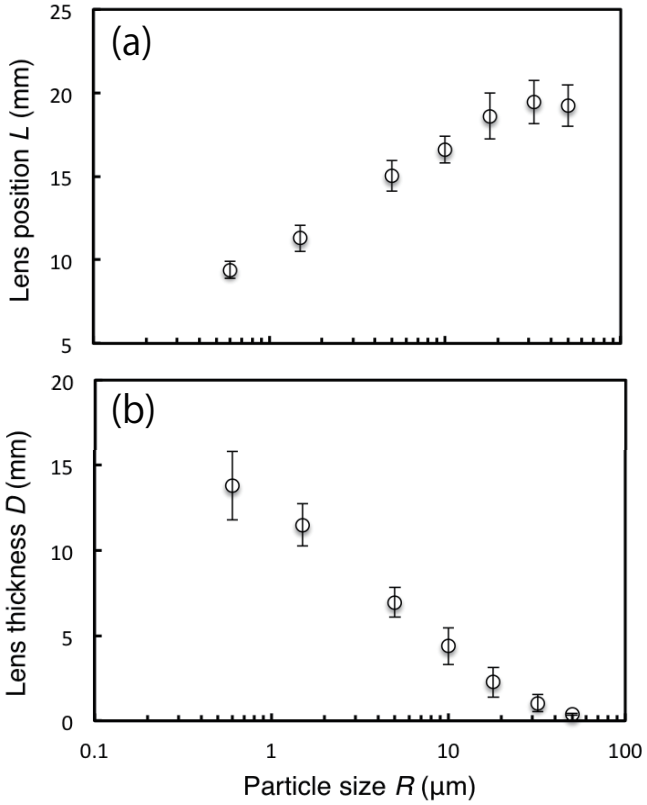

Figure 4.7: Relationships between initiated location (position), growth (thickness) and host particle sizes obtained by freezing experiments. At smaller particles, lens position becomes near from bottom cooling plate (a) and thickness becomes large (b).

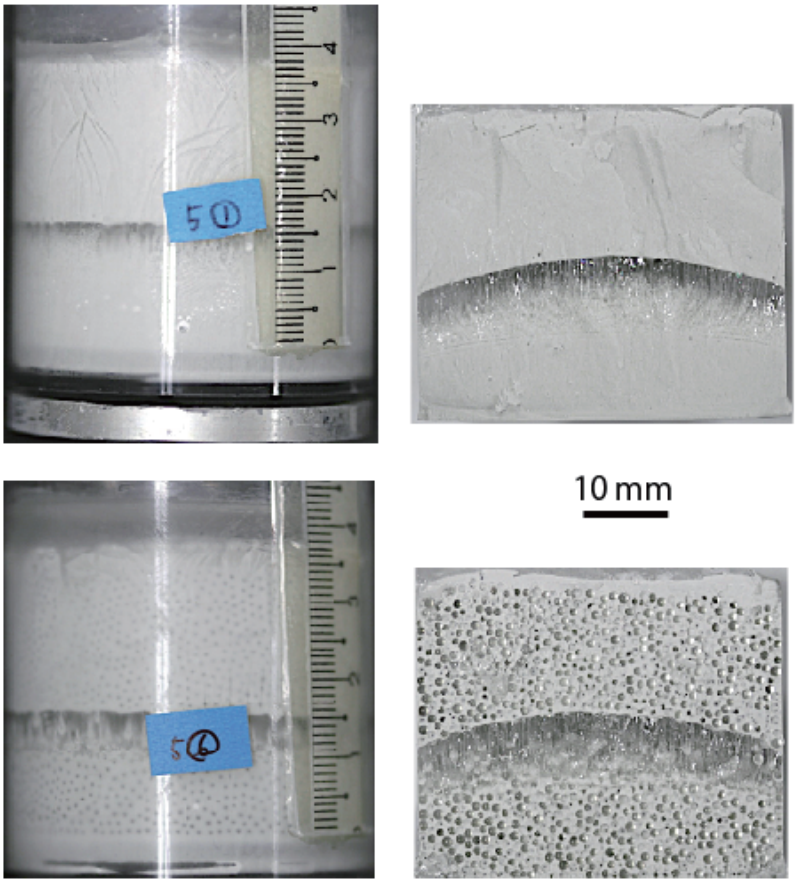

Figure 4.8: Ice lenses in poly-dispersed glass beads. Upper panel is the mixture of 5 μm and 50 μm, while lower panel is of 5 μm and 1000 μm. Both poly-dispersed particles can hold the macroscopic ice lenses despite the presence of large particles.

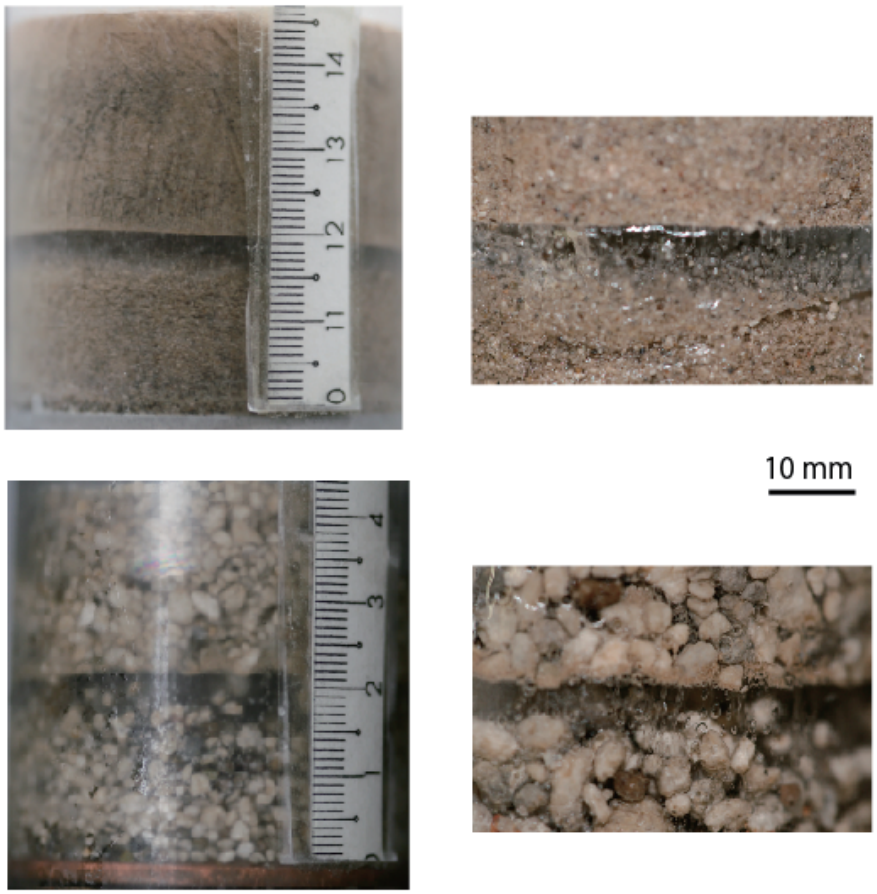

Figure 4.9: Ice lenses in basaltic soils. The particle diameter range is 125–425 μm at upper panel and 1000–4000 μm at lower panel, respectively.

Chapter 5

Modeling and Numerical Calculations

5.1 Overview of This Chapter

This chapter describes the numerical modeling for the ice lens initiation and growth with the thermal diffusion equation in ice-water-particle system and the estimation of liquid thin film thickness. At first I describe the temperature variations to track the growth velocity of the solidification front and the film thickness that is important for lens behaviors. Ice lens growth model is based upon the continuum force-balance model constructed by Rempel et al. [2004]. Schematic diagram of this model is shown in Figure 5.1. Unfrozen region is water-saturated porous media. Water flows as a permeable flow by Darcy's law if pressure difference is imposed. Permeability is a major controlling factor here. This unfrozen region occupies between the top of sediment particle layer and the solidification front. Partially frozen region between unfrozen region and ice lens is a partially-molten region where ice and water coexist. This region corresponds to the frozen fringe proposed by O'Neill and Miller [1985]. This region extends from the freezing front to the ice lens front. Water phase exists as a thin film along the surface of grains. Water can be supplied from this region to the ice lens front through the thin film.

In addition to the Darcy flow, I modified the water flow using Lubrication theory that is referred by Worster and Wettlaufer [1999] and Rempel [2008] as film flow. This term has an important role for the kinetic constraints on the lens growth. Ice lens growth can be subdivided into two regimes with relation to the velocity of freezing front in the porous media. When the freezing velocity is much higher than the growth rate of ice

５章の本文はインターネット公表に関する同意が得られなかったため非公表

Chapter 6

Overall Discussion

6.1 Comparison between the Numerical Predictions and Experiments

6.1.1 Ice Lenses behaviors and Nature of Interactions

Figure 6.1 shows the comparison between numerical predictions and freezing experimental results: (a) shows the initiated location against host particle size and (b) shows the growth thickness after 24 hours of cooling against host particle size. Here the exponent ν gives and indication for the type of interfacial interactions that dominate film behavior: non-retarded van der Waals forces give ν = 3, retarded van der Waals forces give ν = 4, and different limits of electrostatic forces give $\nu \approx 2$ or 3/2. The growth rate V_l drops with the progressive increase in lens temperature and the final thickness D can be compared against the numerically integrated growth-rate predictions. The numerical predictions with ν = 3/2 agree well with the experimental results assuming the equivalent packing conditions and physical properties. This indicates that short-range electrostatic interactions dominate the film behavior in my experimental system. As discussed previous sections, the numerical predictions produce a maximum growth for $\sim$ 1 μm particles and thickness becomes smaller in larger and smaller particles. The maximum results from the low permeability and high resistance to liquid flow around the smaller particles from the water supply above, while the longer path-length for film flow around larger particles increasingly restricts the rate of lens growth for larger particle size.

６章の一部はインターネット公表に関する同意が得られなかったため非公表

deed, the presence of impurities has also been shown to enhance grain-boundary melting [Thomson et al., 2013] that may affect our inferred film thicknesses if significant liquid transport can thereby bypass the growing lens. Without firm constraints on such processes as might be offered by methods to control surface charges, or an enhanced suite of experiments that explores the systematic variation of fluid composition, I view the simple interpretation of our results presented here as the most reasonable at present.

Figure 6.3 (a) compares the positions of ice-lenses predicted by the numerical model (solid line) and experimental results (dots) against host particle size when the film thickness is set to follow a simple power-law $d = d_f(\Delta T_f/\Delta T)^{1/\nu}$ (where d_f and ΔT_f are assigned from the experiments for R = 5 μm) with ν = 1.44. After the macroscopic ice-lens is nucleated at $T_m - \Delta T = T_f$, the rate of heat flow continues to decrease and the rate of lens growth V_l must drop as well, so equation (5.31) requires that ΔT decreases and the temperature on the upper boundary of the lens rises. The changing growth rate V_l can be tracked as the lens temperature and film thickness evolve. Figure 6.3 (b) shows that the measured final thickness D compares favorably with the integrated growth-rate predictions of equation (5.31). A maximum growth is expected for $\sim$ 1 μm particles and D becomes smaller at larger and smaller particle sizes. This maximum results from the low permeability to liquid flow through the finest sediment from the water supply above, while the longer path-length for film flow around larger particles increasingly restricts the rate of lens growth in the coarsest sediments. The maximum growth of the ice lens is determined by the balance between these two restrictions.

6.2 Structures of Ice Lenses

Detailed observations of ice lenses have rarely been performed since the observations should be conducted in the low-temperature environment; and the engineering experiments have not focused on the lens growth but on heaving pressure or amount. Here I argue the structure of ice lenses that observed during the freezing experiments and polarization imaging. Ice lenses obtained by the freezing experiments indicate the convex upward structures as shown in Figure 4.6 with a curvature along the ice lens surface of $\sim$ 3 m^{-1}. Assuming that ice lenses formed along isotherms, this configuration implies a radial temperature gradient and lateral heat flow. Polarization images of sliced ice lenses

for three conditions are shown in Figures 6.4 and 6.5. They show the horizontal and normal planes to the heat flow direction with the particle size of 0.6 μm, salty ice lens (850 ppm) and crashed-basalt, respectively. Vertical planes show the columns of single ice crystals that grow along the heat flow at 0.6 μm particles and basalt. However, the salty ice lens that includes the particle clusters within the grain boundaries does not show the polarization. Normal planes exhibit the clear cross-sections of each single crystals at 0.6 μm and basalt, while the salty lens shows the linear structures. Also the single crystals show the vague configurations.

6.3 Geophysical Applications

6.3.1 Terrestrial Frost Heave Phenomena

Growth of ice lenses causes the upwards displacement of ground surface known as *frost heave*. Beskow's field observations had described the high frost susceptibility of fine-grained particles, but the physical explanation was not provided. Step-wise freezing experiments using homogeneous glass beads demonstrate that the thickness of ice lens becomes larger in finer particles because the lens nucleation occurs at higher freezing velocity and the melting temperature depression becomes larger due to the Gibbs-Thomson effects. In natural environments, the surface temperature shows cyclic daily variations, which leads to the limitation of solidification front advance into the ground. Similar to step-wise freezing, the freezing rate becomes slow at deeper locations and finally approaches zero. Therefore, fine-grained soils such as silt experience large magnitude of frost heaving associated with vigorous growth of ice lenses. This means that the substance (water and soils) transport during freezing is more active in fine-grained soils; and soil holds the massive water or ice near the ground surface. However, when the distance between the ice lens and water reservoir is significantly-long (e.g., the level of ground water is deep), the water flow and ice lens growth are restricted by the resistance of darcy flow due to the low permeability.

Particle size analysis using Peclet number predicts the restriction of the lens growth at sub-micron particles, while natural soils have wide range of size distribution, which induces the spatial heterogeneity of pore-grain structures. To consider the ice lens forma-

tion and frost heave in natural environment, further experiments that incorporate the soils characteristics are required. In the additional experiments, I showed the macroscopic ice lenses in poly-dispersed glass beads and crashed basaltic soils. Although they hold large particles, presence of fine-particles (or size distribution of particles) increases the specific surface area due to the microscopic structures in porous media. In such a case, vigorous frost heaving occurs. Accordingly, the specific surface area is favorable to predict the frost heaving rather than the particle size in natural environments. The total amount of surface heaving is larger than the thickness of macroscopic lens as shown in Figures B.3 and 4.5; therefore, it should be considered that not only macroscopic lens but also invisible lenses or change of packing conditions affect the frost heaving.

6.3.2 Martian Ice Lenses

Existences of unfrozen water and ice in martian near-surface are interesting research objects in terms of the habitability. Considering martian environment that has low temperature and atmospheric pressure, the presence of bulk water is of great difficulty. However, unfrozen water or premelting water can exist in the regolith even below the melting temperature due to the inter-particle interactions. Zent [2008] has estimated that several percent of water can remain in the liquid state at –60 °C. Since martian surface is covered by fine regolith ($\sim$ μm - mm in particle sizes), large surface area can hold the considerable amount of unfrozen water. Beyond the unfrozen water, the nucleations of ice lenses are interested since they require the water supply. If the ice lens initiation and growth occur on martian surface, the patterned ground may be formed by the freeze-thaw cycles and differential frost heaving. Melting of macroscopic ice lens may play a role in bulk water flow and gully formation.

The existence of solute plays an important role about the water behavior since it decreases the melting temperature. Various kinds of salts such as sulfate, chloride and perchlorate are found on the martian surface [e.g., Möhlmann and Thomsen, 2011, Hecht et al., 2009]. Especially, the eutectic temperatures of perchlorate are drastically low [Chevrier et al., 2009] so that liquid water may exist where perchlorate resides in the regolith abundantly. My salty ice lens experiments demonstrate that the solution in pore water displaces the nucleation and growth of ice lenses to lower temperature side. This

transition is enhanced with an increase in solute concentration, while the growth of pure ice layer becomes a difficult due to the trapping of particles into the grain boundaries as shown in Figure C.2. My experiments are performed around the nominal melting temperature; further experiments under much lower temperature environment are required to investigate the effect of solute. Meanwhile, the relationship between the effect of lower atmospheric pressure and role of solute should also be investigated because the electrolytes in water decreases the evaporation rate [Chevrier et al., 2009]. Under dry environments, water vapor diffusion that is ignored in almost previous model (and my experiments) plays a significant role as water source since liquid supply through the regolith pores is not enough and martian atmosphere has vigorous exchanges of substance (such as water vapor, ice, or carbon dioxide) with ground surface.

図６.４，６.５については今後雑誌で公表予定のため非公開

Chapter 7

Conclusions

I have explored the behavior of ice lenses process and the interfacial melting by the unidirectional freezing experiments using homogeneous glass beads and developing the simple continuum model. The comparison of experimental results against numerical predictions suggests the importance of kinetic effects that is ignored in most previous models and the nature of inter-particle interactions. Beyond the simple case of ice lens formation, I developed arguments to the interfacial melting and salt effect.

In the unidirectional freezing experiments, I investigated the position and thickness of ice lenses with changing the host particle size and the induced cooling temperature. As a result of systematic experiments, clear relationships between the host particle sizes, the cooling temperature and ice lens configuration are obtained. The nucleated position of ice lenses becomes further from the cooled boundary with lower cooling temperature. As for the growth thickness, it becomes larger with smaller particle sizes. To compare with the experimental results, I have developed the simple numerical model based upon the continuum model with solving the thermal diffusion equation in ice-water-particle system to track the temperature variations. Comparison between the experimental results and numerical predictions implies the importance of kinetic constraints associated with the lubrication flow around the particle surface. This effect has been ignored in most previous model since the path length is significantly short compared with the Darcy flow in the unfrozen region. In addition, ice lens growth is determined by the balance of permeable flow and film flow, which can be discussed quantitatively using Peclet number that gauges the importance of fluid flow to temperature profile. When the permeable

flow dominates, Peclet number is proportional to particle radius R, which leads to the constraints for the lens growth at fine-grained porous media. By contrast, when the film flow dominates, the Peclet number is inversely proportional to R^3, which reflects the restriction of lens growth in coarse-grained porous media. Therefore, the highest frost susceptibility occurs in intermediate-sized porous media. Beyond the kinetic constraints, the comparisons suggest that the numerical predictions with ν = 3/2 agree well with the experimental results assuming the equivalent packing conditions and physical properties. This indicates that short-range electrostatic interactions dominate the film behavior in my experimental system.

Using the experimentally measured position of ice lenses, I estimated the film thickness at ΔT_f for each particle size and converted to the relationship between the film thickness and temperature depression, which indicates the functional dependence of film thickness on temperature $\nu \approx 1.44$. This value of ν is close to the limiting case expected for short-range electrostatic interactions. In the salty lens experiments, I found substantial differences in behaviors and configurations of ice lenses against the previous experiments. When the pore water includes the salt at high concentrations, ice lens becomes vague and large amount of particle clusters are trapped within the ice grain boundaries. As for the initiation and growth, the nucleated position shifts to lower side with increasing in salt concentrations, while the growth thickness is independent of the concentration.

I used homogeneous glass beads for the freezing experiments and numerical predictions, while natural soils have complicated structures such as local heterogeneity of packing condition, vesiculated surface and size distribution. Therefore further experiments and more accurate numerical treatments that focus on more realistic soil properties and heterogeneity are required to argue the geophysical situations. The constructed physical model can be applied to the intrinsic situations.

PHYSICAL CONSTANTS

C_i	heat capacity of ice	2200 J K^{-1}
C_l	heat capacity of liquid	4200 J K^{-1}
C_p	heat capacity of particle	837 J K^{-1}
e	elementary charge	1.602×10^{-19} C
g	acceleration of gravity	9.8 m s^{-2}
k_b	Boltzmann constant	1.380×10^{-23} J K^{-1}
K_i	thermal conductivity of ice	2.2 W m^{-1} K^{-1}
K_l	thermal conductivity of liquid	0.57 W m^{-1} K^{-1}
K_p	thermal conductivity of particle	1.1 W m^{-1} K^{-1}
K_s	thermal conductivity of surrounding insulation	0.03 W m^{-1} K^{-1}
$\mathcal{L}$	latent heat	3.3×10^5 J kg^{-3}
T_m	bulk melting temperature	273 K
γ_{il}	ice-liquid surface energy	29×10^{-3} J m^{-2}
ϵ_0	dielectric constant of vacuum	8.854×10^{-12} F m^{-1}
μ	dynamic viscosity of water	1.8×10^{-3} Pa s
ρ_i	density of ice	920 kg m^{-3}
ρ_l	density of liquid	1000 kg m^{-3}
ρ_p	density of particle	2600 kg m^{-3}

SYMBOLS

A	Hamaker constant	J
C_o	initial concentration	ppm
C_f	concentration after freezing	ppm
C_{sf}	concentration at solidification front after freezing	ppm
C_i	heat capacity of ice	J K^{-1}
C_l	heat capacity of liquid	J K^{-1}
C_p	heat capacity of particle	J K^{-1}
D	thickness of ice lens	mm
D_c	diameter of chamber	m
δ_D	diffusion length	m
d	film thickness	m
e	elementary charge	C
G_{qll}	Gibbs free energy of quasi-liquid layer	J
f	geometrical parameter	-
F	Helmholtz free energy	J
F_v	van der Waals force per unit area	N m^{-2}
$F(d)$	interfacial potential	J
$f(d)$	film contribution to potential	-
g	acceleration of gravity	m s^{-2}
H	radial heat transfer coefficient	W m^{-2} K^{-1}
h	distance between two planar surface	m
h_s	thickness of surrounding insulation	m
k_0	permeability	m^2
k	equilibrium distribution constant	-
k_b	Boltzmann constant	J K^{-1}
K_i	thermal conductivity of ice	W m^{-1} K^{-1}
K_l	thermal conductivity of liquid	W m^{-1} K^{-1}
K_p	thermal conductivity of particle	W m^{-1} K^{-1}
K_{e0}	water-saturated thermal conductivity	W m^{-1} K^{-1}

K_{e-}	thermal conductivity of ice-water-particle	W m^{-1} K^{-1}
K_s	thermal conductivity of surrounding insulation	W m^{-1} K^{-1}
$\mathcal{K}$	curvature of particle	m^{-1}
L	position of ice lens	mm
L_t	location of upper boundary of ice lens	mm
$\mathcal{L}$	latent heat	J kg^{-3}
n	nature of dominant interactions coefficient	-
Pe	Peclet number	N m^{-2}
p_f	pressure scale	-
p_p	inter-particle pressure	Pa m^{-1}
p_T	thermomolecular pressure	N m^{-2}
R	particle radius	m
R_p	pore throat radius	m
S	Stefan number	-
s_i	specific entropy of ice	J K^{-1}
s_l	specific entropy of liquid	J K^{-1}
T	temperature	K (or °C)
ΔT_f	depression of melting temperature	K (or °C)
$T_{\max}$	temperature at $z_{\max}$	K (or °C)
T_m	bulk melting temperature	K (or °C)
T_{ex}	exterior temperature	K (or °C)
T_0	induced cooling temperature	K (or °C)
T_l	lens temperature	K (or °C)
T_u	upper lens temperature after freezing	K (or °C)
t	elapsed time	s
V_f	lens growth rate at first stage	m s^{-1} (or μm s^{-1})
V_l	lens growth rate at second stage	m s^{-1} (or μm s^{-1})
w	overburden scale	-
Z	valence of the ion	-
z	vertical coordinate	m
$z_{\max}$	top of sediment column	m
z_{T0}	initial upper boundary of sediments	m

z_T	upper boundary of sediments	m
z_l	upper boundary of ice lens	m
z_f	location of the depressed melting point	m
$\mathcal{Z}$	interaction constant	J m^{-1}
α	pore throat scale	-
Γ	ratio of the volumetric heat capacities of fluid and porous media	-
γ_{il}	ice-liquid surface energy	J m^{-2}
$\Delta\gamma$	surface energy difference	J m^{-2}
ϵ	relative dielectric constant of material	-
ϵ_0	dielectric constant of vacuum	F m^{-1}
ζ	film term scale	-
η	viscosity in liquid film	Pa s
κ	inverse of Debye-length	m^{-1}
κ_e	effective thermal diffusivity	m^2 s^{-1}
κ_ν	factor of pressure dependence of T_m	-
Λ	prefactor of ice-liquid-particle interactions	J
λ	characteristic film thickness	m
$\lambda_\mathcal{K}$	characteristic film thickness with curvature	m
μ	dynamic viscosity of water	Pa s
μ'	relative viscosity of film water	-
μ_i	chemical potential of ice	J
μ_l	chemical potential of bulk water	J
$\Delta\mu$	chemical potential difference between ice and bulk liquid	J
ν	functional dependence on temperature	-
ξ	stretched coordinate	-
ρ_i	density of ice	kg m^{-3}
ρ_l	density of liquid	kg m^{-3}
ρ_p	density of particle	kg m^{-3}
σ	surface charge density	C m^{-2}
σ_m	constant of molecular diameter	m
ϕ	porosity	-
ψ	electrical potential	V

Appendix Aについては共著者の同意が得られていないため，非公開

Appendix B についてはインターネット公表に関する同意が得られなかったため非公表

Appendix C，Dについては今後雑誌で公表予定のため非公開

Bibliography

Andersland, O. B. and B. Ladanyi. *An Introduction to Frozen Ground Engineering*. Chapman and Hall, 2nd edition, 2004.

Anderson, A. M. and M. G. Worster. Periodic ice banding in freezing colloidal dispersions. *Langmuir*, 28(48):16512–16523, 2012.

Anderson, D. M. and N. R. Morgenstern. *Permafrost. Proceedings of Second International Conference*. National Academy of Science, 257–288, 1973.

Anderson, R. S. and S. P. Anderson. *Geomorphology : The Mechanics and Chemistry of Landscapes*. Cambridge University Press, 2010.

Azmatch, T. F., D. C. Sego, L. U. Arenson, and K. W. Biggar. New ice lens initiation condition for frost heave in fine-grained soils. *Cold Regions Science and Technology*, 82:8–13, 2012.

Baker, M. B. and J. G. Dash. Charge transfer in thunderstorms and the surface melting of ice. *Journal of Crystal Growth*, 97:770–776, 1989.

Beskow, G. *Soil Freezing and Frost Heaving with Special Application to Roads and Railroads*. Technological Institute, (Northwestern University), 1935. [Reprinted 1991 CRREL Spec. Rep. 91-23, 37-157].

Cahn, J. W., J. G. Dash, and H. Y. Fu. Theory of ice premelting in monosized powders. *Journal of Crystal Growth*, 123(1-2):101–108, 1992.

Chevrier, V. F., J. Hanley, and T. S. Altheide. Stability of perchlorate hydrates and their liquid solutions at the Phoenix landing site, Mars. *Geophysical Research Letters*, 36: L10202, 2009.

Corte, A. E. Vertical migration of particles in front of a moving freezing plane. *Journal of Geophysical Research*, 67(3):1085–1090, 1962.

Dash, J. G. Surface melting. *Contemporary Physics*, 30:89–100, 1989.

Dash, J. G., H. Y. Fu, and J. S. Wettlaufer. The premelting of ice and its environmental consequences. *Reports on Progress in Physics*, 58(1):115–167, 1995.

Dash, J. G., A. W. Rempel, and J. S. Wettlaufer. The physics of premelted ice and its geophysical consequences. *Reviews Modern Physics*, 78(3):695–741, 2006.

Elbaum, M., S. G. Lipson, and J. G. Dash. Optical study of surface melting on ice. *Journal of Crystal Growth*, 129:491–505, 1993.

Elliott, J. A. W. and S. S. L. Peppin. Particle trapping and banding in rapid colloidal solidification. *Physical Review Letters*, 107(16):168301, 2011.

Engemann, S., H. Reichert, H. Dosch, J. Bilgram, V. Honkimäki, and A. Snigirev. Interfacial melting of ice in contact with SiO_2. *Physical Review Letters*, 92(20):205701, 2004.

Everett, D. H. The thermodynamics of frost damage to porous solids. *Transactions of the Faraday Society*, 57:1541–1551, 1961.

Ewing, G. E. Thin film water. *Journal of Physical Chemistry B*, 108(41):15953–15961, 2004.

French, H. M. *The Periglacial Environment*. John Wiley & Sons, Ltd., 3rd edition, 2007.

Furukawa, Y. and H. Nada. Anisotropic surface melting of an ice crystal and its relationship to growth forms. *Journal of Physical Chemistry B*, 101(32):6167–6170, 1997.

Gilpin, R. R. A model of the "liquid-like" layer between ice and a substrate with applications to wire regelation and particle migration. *Journal of Colloid and Interface Science*, 68(2):235–251, 1979.

Gilpin, R. R. Wire regelation at low temperatures. *Journal of Colloid and Interface Science*, 77(2):435–448, 1980.

Hansen-Goos, H. and J. S. Wettlaufer. Theory of ice premelting in porous media. *Physical Review E*, 81:031604, 2010.

Hecht, M. H., S. P. Kounaves R. C. Quinn, S. J. West, S. M. M. Young, D. W. Ming, D. C. Catling, B. C. Clark, W. V. Boynton, J. Hoffman, L. P. DeFlores, K. Gospodinova, J. Kapit, and P. H. Smith. Detection of perchlorate and the soluble chemistry of martian soil at the Phoenix lander site. *Science*, 325:64–67, 2009.

Hiroi, M., T. Mizusaki, T. Tsuneto, A. Hirai, and K. Eguchi. Frost-heave phenomena of ^{4}He on porous glasses. *Physical Review B*, 40(10):6581–6590, 1989.

Ishizaki, T., M. Maruyama, Y. Furukawa, and J. G. Dash. Premelting of ice in porous silica glass. *Journal of Crystal Growth*, 163(4):455–460, 1996.

Israelachvili, J. N. *Intermolecular and surface forces: revised third edition*. Academic press, 2011.

Konrad, J. M. Estimation of the segregation potential of fine-grained soils using the frost heave response of two reference soils. *Canadian Geotechnical Journal*, 42:38–50, 2005.

Konrad, J. M. and N. R. Morgenstern. The segregation potential of freezing soil. *Canadian Geotechnical Journal*, 18:482–491, 1981.

Kuroda, T. Theoretical study of frost heaving – kinetic process at water layer between ice lens and soil particles. In *Proceedngs of Fourth International Symposium on Ground Freezing*, pages 5–7, 1985.

Levy, J. S., D. R. Marchant, and J. W. Head. Thermal contraction crack polygons on Mars: A synthesis from HiRISE, Phoenix, and terrestrial analog studies. *Icarus*, 206: 229–252, 2010.

Lipp, G. and C. Körber. On the engulfment of spherical-particles by a moving ice liquid interface. *Journal of Crystal Growth*, 130(3-4):475–489, 1993.

Mader, H. M. Observations of water-vein system in polycrystalline ice. *Journal of Glaciology*, 38(130):333–347, 1992.

Mashl, S. J., R. A. Flores, and R. Trivedi. Dynamics of solidification in 2% corn starch water mixtures: Effect of variations in freezing rate on product homogeneity. *Journal of Food Science*, 61(4):760–765, 1996.

Mellon, M. T., R. E. Arvidson, J. J. Marlow, R. J. Phillips, and E. Asphaug. Periglacial landforms at the Phoenix landing site and the northern plains of Mars. *Journal of Geophysical Research*, 113:E00A23, 2008.

Mellon, M. T., R. E. Arvidson, H. G. Sizemore, M. L. Searls, D. L. Blaney, S. Cull, M. H. Hecht, T. L. Heet, H. U. Keller, M. T. Lemmon, W. J. Markiewicz, D. W. Ming, R. V. Morris, W. T. Pike, and A. P. Zent. Ground ice at the Phoenix Landing Site: Stability state and origin. *Journal of Geophysical Research*, 114:E00E07, 2009.

Miller, R. D. Freezing and heaving of saturated and unsaturated soils. *Highway Research Record*, 393:1–11, 1972.

Miller, R. D. Frost heaving in non-colloidal soils. In *Proceedings of third International Conference on Permafrost*, volume 1, pages 708–713, 1978.

Mizusaki, T., R. Nomura, and M. Hiroi. Growth rate of frost heave in helium and mass transport in solid ^{4}He. *Journal of Low Temperature Physics*, 149(3-4):143–150, 2007.

Möhlmann, D. and K. Thomsen. Properties of cryobrines on Mars. *Icarus*, 212:123–130, 2011.

Murton, J. B., R. Peterson, and J. C. Ozouf. Bedrock fracture by ice segregation in cold regions. *Science*, 314:1127–1129, 2006.

Mutou, Y., K. Watanabe, T. Ishizaki, and M. Mizoguchi. Microscopic observation of ice lensing and frost heaves in glass beads. In *Proceedings of Seventh International Conference on Permafrost*, pages 283–287, 1998.

Nada, H. and Y. Furukawa. Anisotropy in molecular-scaled growth kinetics at ice-water interfaces. *Journal of Physical Chemistry B*, 101:6163–6166, 1997.

Nagashima, K., T. Suzuki, M. Nagamoto, and T. Shimizu. Formation of periodic layered pattern of tetrahydrofuran clathrate hydrates in porous media. *Journal of Physical Chemistry B*, 112(32):9876–9882, 2008.

Nye, J. F. The geometry of water veins and nodes in polycrystalline ice. *Journal of Glaciology*, 35(119):17–22, 1989.

Obata, M. and N. Nagahara. Layering of alpine-type peridotite and the segregation of partial melt in the upper mantle. *Journal of Geophysical Research*, 92(B5):3467–3474, 1987.

O'Neill, K. and R. D. Miller. Exploration of a rigid ice model of frost heave. *Water Resources Research*, 21(3):281–296, 1985.

Peppin, S. S. L., J. S. Wettlaufer, and M. G. Worster. Experimental verification of morphological instability in freezing aqueous colloidal suspensions. *Physical Review Letters*, 100(23):238301, 2008.

Peterson, R. A. Assessing the role of differential frost heave in the origin of non-sorted circles. *Quaternary Research*, 75:325–333, 2011.

Peterson, R. A. and W. B. Krantz. A mechanism for differential frost heave and its implications for patterned ground formation. *Journal of Glaciology*, 49:69–80, 2003.

Peterson, R. A. and W. B. Krantz. Differential frost heave model for patterned ground formation: Corroboration with observations along a North American arctic transect. *Journal of Geophysical Research*, 113:G03S04, 2008.

Rempel, A. W. Formation of ice lenses and frost heave. *Journal of Geophysical Research*, 112:F02S21, 2007.

Rempel, A. W. A theory for ice-till interactions and sediment entrainment beneath glaciers. *Journal of Geophysical Research*, 113:F01013, 2008.

Rempel, A. W. Hydromechanical processes in freezing soils. *Vadose Zone Journal*, 11: doi:10.2136/vzj2012.0045, 2012.

Rempel, A. W. and M.G. Worster. The interaction between a particle and an advancing solidification front. *Journal of Crystal Growth*, 205:427–440, 1999.

Rempel, A. W., J. S. Wettlaufer, and M. G. Worster. Interfacial premelting and the thermomolecular force: Thermodynamic buoyancy. *Physical Review Letters*, 87(8):088501, 2001a.

Rempel, A. W., E. D. Waddington, J. S. Wettlaufer, and M. G. Worster. Possible displacement of the climate signal in ancient ice by premelting and anomalous diffusion. *Nature*, 411(8):568–571, 2001b.

Rempel, A. W., J. S. Wettlaufer, and M. G. Worster. Premelting dynamics in a continuum model of frost heave. *Journal of Fluid Mechanics*, 498:227–244, 2004.

Roller, P. S. The bulking properties of microscopic particles. *Industrial & Engineering Chemistry Research*, 22(11):1206–1208, 1930.

Sadtchenko, V. and G. E. Ewing. Interfacial melting of thin ice films: An infrared study. *Journal of Chemical Physics*, 116(11):4686–4697, 2002.

Saruya, T., K. Kurita, and A. W. Rempel. Experimental constraints on the kinetics of ice lens initiation and growth. *Physical Review E*, 87(3):032404, 2013.

Saruya, T., A. W. Rempel, and K. Kurita. Indirect measurement of interfacial melting from macroscopic ice observations. *Physical Review E*, 89(6):060401(R), 2014a.

Saruya, T., A. W. Rempel, and K. Kurita. Hydrodynamic transitions with changing particle size that control ice lens growth. *Journal of Physical Chemistry B*, 118, 13420–13426, 2014b.

Schöder, S., H. Reichert, H. Schröder, M. Mezger, J. S. Okasinski, V. Honkimäki, J. Bilgram, and H. Dosch. Radiation-induced premelting of ice at silica interfaces. *Physical Review Letters*, 103(9):095502, 2009.

Shean, D. E., J. W. Head, and D. R. Marchant. Origin and evolution of a cold-based tropical mountain glacier on Mars: The Pavonis Mons fan-shaped deposit. *Journal of Geophysical Research*, 110:E05001, 2005.

Sizemore, H. G., A. P. Zent, and A. W. Rempel. Initiation and growth of martian ice lenses. *Icarus*, (in press), 2014.

Smith, P. H., L. K. Tamppari, R. E. Arvidson, D. Bass, D. Blaney, W. V. Boynton, A. Carswell, D. C. Catling, B. C. Clark, T. Duck, E. DeJong, D. Fisher, W. Goetz, H. P. Gunnlaugsson, M. H. Hecht, V. Hipkin, J. Hoffman, S. F. Hviid, H. U. Keller, S. P. Kounaves, C. F. Lange, M. T. Lemmon, M. B. Madsen, W. J. Markiewicz, J. Marshall, C. P. McKay, M. T. Mellon, D. W. Ming, R. V. Morris, W. T. Pike, N. Renno, U. Staufer, C. Stoker, P. Taylor, J. A. Whiteway, and A. P. Zent. H_2O at the Phoenix Landing Sites. *Science*, 325:58–61, 2009.

Spaans, E. J. A. and J. M. Baker. Examining the use of time domain reflectometry for measuring liquid water content in frozen soil. *Water Resources Research*, 31(12):2917–2925, 1995.

Style, R. W. and S. S. L. Peppin. The kinetics of ice-lens growth in porous media. *Journal of Fluid Mechanics*, 692:482–498, 2012.

Style, R. W., S. S. L. Peppin, A. C. F. Cocks, and J. S. Wettlaufer. Ice-lens formation and geometrical supercooling in soils and other colloidal materials. *Physical Review E*, 84 (4):041402, 2011.

Taber, S. Frost heaving. *Journal of Geology*, 37:428–461, 1929.

Taber, S. Exploration of a rigid ice model of frost heave. *Journal of Geology*, 38:303–317, 1930.

Takahashi, N. Evidence for melt segregation towards fractures in the Horoman mantle peridotite complex. *Nature*, 359:52–55, 1992.

Takazawa, E., F. A. Frey, N. Shimizu, A. Saal, and M. Obata. Polybaric petrogenesis of magic layers in the Horoman peridotite complex, Japan. *Journal of Petrology*, 40(12): 1827–1851, 1999.

Thomson, E. S., H. Hansen-Goos, J. S. Wettlaufer, and L. A. Wilen. Grain boundary melting in ice. *Journal of Chemical Physics*, 138:124707, 2013.

Toramaru, A. and N. Fujii. Connectivity of melt phase in a partially molten peridotite. *Journal of Geophysical Research*, 91(B9):9239–9252, 1986.

Toramaru, A., E. Takazawa, T. Morishita, and K. Matsukage. Model of layering formation in a mantle peridotite (Horoman, Hokkaido, Japan). *Earth and Planetary Science Letters*, 185:299–313, 2001.

Torrance, J. K. and F. J. Schellekens. Chemical factors in soil freezing and frost heave. *Polar Record*, 42(220):33–42, 2006.

Watanabe, K. Relationship between growth rate and supercooling in the formation of ice lenses in a glass powder. *Journal of Crystal Growth*, pages 237–239, 2002.

Watanabe, K. and M. Mizoguchi. Ice configuration near a growing ice lens in a freezing porous medium consisting of micro glass particles. *Journal of Crystal Growth*, 213 (1-2):135–140, 2000.

Weast, R. C. *CRC Handbook of Chemistry and Physics, 64th ed.* CRC Press, 1984.

Werner, B. T. and B. Hallet. Numerical simulation of self-organized stone stripes. *Nature*, 361:142–145, 1993.

Wettlaufer, J. S. Impurity effects in the premelting of ice. *Physical Review Letters*, 76: 3602–3605, 1999.

Wettlaufer, J. S. and M. G. Worster. Dynamics of premelted films: Frost heave in a capillary. *Physical Review E*, 51:4679–4689, 1995.

Wettlaufer, J. S., M. G. Worster, L. A. Wilen, and J. G. Dash. A theory of premelting dynamics for all power law forces. *Physical Review Letters*, 76(19):3602–3605, 1996.

Wettlaufer, J. S., M. G. Worster, and L. A. Wilen. Premelting dynamics: Geometry and interactions. *Journal of Physical Chemistry B*, 101(32):6137–6141, 1997.

Wilen, L. A. and J. G. Dash. Frost heave dynamics at a single-crystal interface. *Physical Review Letters*, 74(25):5076–5079, 1995a.

Wilen, L. A., J. S. Wettlaufer, M. Elbaum, and M. Schick. Dispersion-force effects in interfacial premelting of ice. *Physical Review B*, 52(16):12426–12433, 1995b.

Worster, M. G. and J. S. Wettlaufer. The fluid mechanics of premelted liquid films. In W. Shyy and R. Narayanan, editors, *Fluid Dynamics at Interfaces*, pages 339–351. Cambridge University Press, 1999.

Zent, A. A historical search for habitable ice at the Phoenix landing site. *Icarus*, 196: 385–408, 2008.

Zhu, D. M., O. E. Vilches, J. G. Dash, B. Sing, and J. S. Wettlaufer. Frost heave in argon. *Physical Review Letters*, 85(23):4908–4911, 2000.